

# Calculated Coupling of Electron and Proton Transfer in the Photosynthetic Reaction Center of *Rhodopseudomonas viridis*

C. Roy D. Lancaster,\* Hartmut Michel,\* Barry Honig,<sup>†</sup> and M. R. Gunner<sup>§</sup>

\*Max-Planck-Institut für Biophysik, Abteilung Molekulare Membranbiologie, D-60528 Frankfurt am Main, Germany; <sup>†</sup>Department of Biochemistry and Molecular Biophysics, Columbia University, New York, New York 10032 USA, and <sup>§</sup>Department of Physics, City College of New York, New York, New York 10031 USA

**ABSTRACT** Based on new *Rhodopseudomonas (Rp.) viridis* reaction center (RC) coordinates with a reliable structure of the secondary acceptor quinone ( $Q_B$ ) site, a continuum dielectric model and finite difference technique have been used to identify clusters of electrostatically interacting ionizable residues. Twenty-three residues within a distance of 25 Å from  $Q_B$  ( $Q_B$  cluster) have been shown to be strongly electrostatically coupled to  $Q_B$ , either directly or indirectly. An analogous cluster of 24 residues is found to interact with  $Q_A$  ( $Q_A$  cluster). Both clusters extend to the cytoplasmic surface in at least two directions. However, the  $Q_B$  cluster differs from the  $Q_A$  cluster in that it has a surplus of acidic residues, more strong electrostatic interactions, is less solvated, and experiences a strong positive electrostatic field arising from the polypeptide backbone. Consequently, upon reduction of  $Q_A$  or  $Q_B$ , it is the  $Q_B$  cluster, and not the  $Q_A$  cluster, which is responsible for substoichiometric proton uptake at neutral pH. The bulk of the changes in the  $Q_B$  cluster are calculated to be due to the protonation of a tightly coupled cluster of the three Glu residues (L212, H177, and M234) within the  $Q_B$  cluster. If the lifetime of the doubly reduced state  $Q_B^{2-}$  is long enough, Asp M43 and Ser L223 are predicted to also become protonated. The calculated complex titration behavior of the strongly interacting residues of the  $Q_B$  cluster and the resulting electrostatic response to electron transfer may be a common feature in proton-transferring membrane protein complexes.

## GLOSSARY

D	primary electron donor (special pair)
$\Delta\Delta G_{rxn}$	"desolvation penalty" (= difference in reaction field energy for residue $i$ in solution and in the protein)
$\Delta G_{crg}(i,j)$	interaction energy between ionizable residues $i$ and $j$ when both are ionized
$\Delta G_{pol}$	contribution of polypeptide backbone and polar side chains to the electrostatic energy experienced by residue $i$
$\Delta pK_{desolv}$	pK shift arising from the "desolvation penalty," $\Delta\Delta G_{rxn}$
$\Delta pK_{pol}$	pK shift arising from polar energy term, $\Delta G_{pol}$
N	number of ionizable sites in a protein
$\phi$	bacteriopheophytin
$pK_a$	pH value at which the average (fractional) protonation $\langle x_i \rangle = 0.5$
$pK_{int}$	the $pK_a$ for an ionizable group in a protein if all other groups were neutral, $= pK_{sol} - c_a (\Delta pK_{desolv} + \Delta pK_{pol})$ ; with $c_a = 1$ for basic residues (Arg, His, Lys, amino terminus, Ser L223), $c_a = -1$ for acidic residues (Asp, carboxy terminus, Glu, Pra, Prd)
$pK_{sol}$	$pK_a$ for an ionizable amino acid side chain in aqueous solution
Pra, Prd	heme propionates
$Q_A$	primary quinone
$Q_B$	secondary quinone
$x$	protonation state of protein
$x_i$	protonation state of ionizable amino acid residue $i$

The three-letter amino acid code (IUPAC-IUB, 1984) and standard nomenclature of quinones with isoprenoid side chains (IUPAC-IUB, 1975) are used throughout.

## Interconversion of energy units

1 kcal/mol	= 4.184 kJ/mol
1 $\Delta pK$ unit	= 1.38 kcal/mol
1 kT	= 0.59 kcal/mol = 0.43 $\Delta pK$ units
1 eV	= 23.06 kcal/mol = 16.71 $\Delta pK$ units

## INTRODUCTION

A fundamental principle in bioenergetics is the coupling of electron transfers to the translocation of protons through proteins embedded in the energy-transducing cellular membranes. In bacterial photosynthesis, proton uptake from the cytoplasm is coupled to light-induced electron transfer in photosynthetic reaction centers (RCs). The RCs from purple bacteria are the best-characterized membrane proteins. The crystal structure of the RC from the nonsulfur purple bacterium *Rhodopseudomonas (Rp.) viridis* was the first integral membrane protein structure to be determined at atomic resolution (Deisenhofer et al., 1985; Deisenhofer and Michel, 1989). It is composed of four polypeptides (the L, M, and H subunits and a tightly bound cytochrome *c*) and 14 cofactors (four hemes, four bacteriochlorophyll-*b*, two bacteriopheophytin-*b*, one nonheme iron, two quinones, and one carotenoid). The complex has 11 membrane-spanning helices: five in the L, five in the M, and one in the H subunit. Large parts of the L and M subunits and their associated cofactors are related by a twofold symmetry axis perpendicular to the plane of the membrane. This membrane protein complex plays a central role in the conversion of light energy into chemical energy (Nicholls and Ferguson, 1992). The absorption of a photon by a dimer of bacteriochlorophyll, the so-called special pair D (we use the nomenclature proposed by Hoff, 1988) leads to a charge

Received for publication 28 November 1995 and in final form 15 February 1996.

Address reprint requests to Dr. Hartmut Michel, Max-Planck-Institut für Biophysik, Abteilung Molekulare Membranbiologie, Heinrich-Hoffmann-Str. 7, D-60528 Frankfurt am Main, Germany. Tel.: 49-69-96769-401; Fax: 49-69-96769-423; E-mail: michel@mpibp-frankfurt.mpg.de.

© 1996 by the Biophysical Society

0006-3495/96/06/2469/24 \$2.00

separation between D and the menaquinone,  $Q_A$ , bound to the M subunit (reviewed by Kirmaier and Holten, 1993; Zinth and Kaiser, 1993). The electron is then transferred from  $Q_A$  to a secondary quinone,  $Q_B$ , bound to the L subunit (reviewed by Parson, 1978; Shinkarev and Wraight, 1993). After a second reduction of  $Q_B$  and the uptake of two protons from the cytoplasm, the ubiquinol ( $Q_BH_2$ ) leaves its binding site (Crofts and Wraight, 1983; McPherson et al., 1990) and is reoxidized by a second membrane protein complex, the cytochrome  $bc_1$  complex (cf. Knaff, 1993, for a review), which results in the release of protons on the periplasmic side of the membrane. This proton transport produces a transmembrane electrochemical gradient that drives ATP synthesis through a third membrane-spanning complex, the ATP synthase (Mitchell, 1979). In summary, the reduction of bound  $Q_B$  to the quinol associated with the uptake of protons into the RC is an important step in the energetics of photosynthetic bacteria (Cramer and Knaff, 1991).

The sequence of light-induced electron and proton transfer reactions that occur within the RC in the process of reducing  $Q_B$  to  $Q_BH_2$  has been represented by a quinone reduction cycle (Okamura and Feher, 1992; Fig. 1). The cycle starts with the RC in the initial state  $DQ_AQ_B$ . Light absorption leads to an excited primary donor  $D^*$ , from which an electron is transferred via the monomeric bacteriochlorophyll  $B_A$  and the bacteriopheophytin  $\phi_A$  to  $Q_A$  in 200 ps (Parson and Ke, 1982; Holzapfel et al., 1989), leading to the formation of  $D^+Q_A^-Q_B$ . Re-reduction of  $D^+$  by cytochrome  $c_{558.5}$  (heme 3; Fritzsch et al., 1989) occurs in 320 ns (Dracheva et al., 1988). These processes are much faster than the subsequent proton uptake and inter-quinone electron transfer reactions. Therefore, the first step of quinone reduction in *Rp. viridis* RCs can be viewed as a photochemical cytochrome oxidation, giving rise to the radical state  $DQ_A^-Q_B$ . The second step involves the transfer of this first electron to  $Q_B$  (in 17–25  $\mu$ s; Carithers and

Parson, 1975; Leibl and Breton, 1991; Mathis et al., 1992), resulting in the state  $DQ_AQ_B^-$ . After a second photochemical cytochrome oxidation in the third step, the diradical state  $DQ_A^-Q_B^-$  is formed. The fourth step results in the singly protonated, doubly reduced state  $DQ_A(Q_BH)^-$  and could proceed through two possible paths. Either proton uptake could be followed by transfer of the second electron, involving an intermediate state  $DQ_A^-Q_BH$ , or electron transfer could lead to the intermediate state  $DQ_AQ_B^{2-}$  and then be followed by proton transfer. Deduction of free energy changes associated with the formation of  $Q_BH_2$  in native and Glu L212 → Gln mutant RCs from *Rb. sphaeroides* favored the intermediate state  $DQ_AQ_B^{2-}$  (McPherson et al., 1994). However, this is clearly not an equilibrium state, because  $Q_B^{2-}$  will be rapidly doubly protonated. Nevertheless, this redox state was included in the present analysis, first because it is a possible intermediate and second because sites that are calculated to bind protons in the presence of  $Q_B^{2-}$  may be good candidates for sites that can be transiently protonated and serve as proton donors to  $Q_B^-$  in the  $DQ_A^-Q_B^-$  state. The transfer of the second proton to  $Q_BH^-$  (step 5 in Fig. 1) is kinetically indistinguishable from the first proton transfer in the wild-type RC and can only be resolved in the case of mutants with significantly retarded second proton transfer rates (McPherson et al., 1994).

Both  $Q_A$  and  $Q_B$  sites are deeply buried within the reaction center complex, approximately 15 Å from the cytoplasmic surface. After the initial reduction of  $Q_A$  and  $Q_B$ , protons are bound to protonatable residues within the protein. In addition, after the second reduction of  $Q_B$ , the release of the product quinol requires proton transfer to the reduced quinone within the  $Q_B$ -binding site. This could occur by protons moving along a chain of proton donors and acceptors by a "proton wire" or hydrogen-bonded chain mechanism (Nagle and Tristam-Nagle, 1983). Possible proton donors and acceptors are protonatable amino acid residues and water molecules. The challenge is to assign the changes in protonation of the protein to specific residues. A number of the protonatable residues between the  $Q_B$  site and the cytoplasmic surface have been shown to be functionally relevant for the proton transfer process by analysis of site-directed mutations (reviewed by Okamura and Feher, 1992, 1995; Takahashi and Wraight, 1994) and second site revertants (Hanson et al., 1993; reviewed by Sebban et al., 1995a). The observed effects can be due to modification of the kinetics or thermodynamics of electron or proton transfer. Identification of residues that contribute to the changes in equilibrium distributions of protons in the different redox states of the protein should help to determine the role of the functionally important residues.

Recent advances in structure-based electrostatic calculations (reviewed by Honig and Nicholls, 1995; cf. also Warwicker and Watson, 1982; Warshel and Russel, 1984; Harvey, 1989; Sharp and Honig, 1990) on the RCs of *Rb. sphaeroides* (Beroza et al., 1991; Gunner and Honig, 1992; Beroza et al., 1995) and *Rp. viridis* (Cometta-Morini et al.,

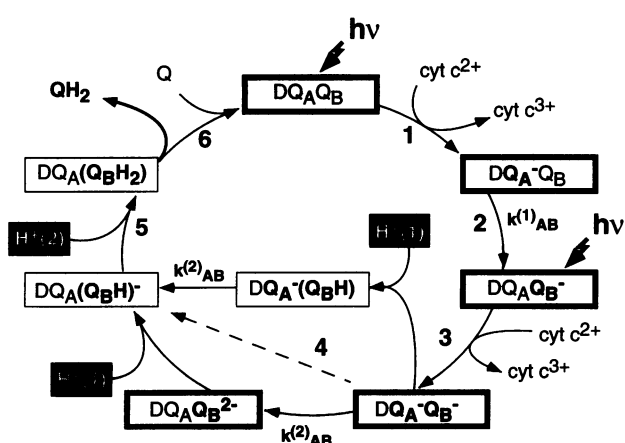


FIGURE 1 Quinone reduction cycle (modified from Okamura and Feher, 1992). Reduced quinones are typeset in bold. Steps 2, 4, 5, and 6 are reversible. Bold frames highlight the five redox states studied in the present work. See text for details.

1993) have demonstrated the ability of this method to provide insight into the coupling of proton transfer to electron transfer. These studies were restricted to the "neutral" RC, i.e., the ground-state  $DQ_AQ_B$ , and to the redox state after the transfer of the first electron to  $Q_A$  or  $Q_B$ . Furthermore, these calculations were based on structures with  $Q_B$  sites that were either weakly defined (as was the case for the *Rp. viridis* RC) or that display significant discrepancies in the  $Q_B$  site of independently determined structures (as is the case for the *Rb. sphaeroides* RC structures; Lancaster et al., 1995). A more reliable  $Q_B$  site structure has been obtained from x-ray crystallographic analysis of crystals that have full occupancy of ubiquinone-2 in the  $Q_B$  site of the *Rp. viridis* RC (Lancaster and Michel, manuscript in preparation; Lancaster and Michel, 1996). Based on this new structure, we have used a continuum dielectric model and finite difference technique to identify clusters of electrostatically interacting ionizable residues and calculate the average protonation of ionizable residues in the five redox states: the ground state,  $Q_A^-$ ,  $Q_B^-$ ,  $Q_A^-Q_B^-$ , and  $Q_AQ_B^{2-}$ . The results are compared to those obtained earlier on *Rb. sphaeroides* RCs and to experimental data.

## MATERIALS AND METHODS

### Coordinates

The nonhydrogen atom coordinates of the *Rp. viridis* reaction center structure based on  $Q_B$  reconstitution with ubiquinone-2 (Lancaster and Michel, manuscript in preparation) were used in the calculations. Protons were added with the programs HPP and PROTEUS (A. Joguine and M. R. Gunner, City College of New York, unpublished). HPP adds those protons that are uniquely determined by heavy atom positions. PROTEUS orients the positions of protons on water molecules and hydroxyl groups to minimize the electrostatic interaction free energy of the proton with residues within 4.5 Å of the hydroxyl or water oxygen. Sulfate, detergent, and water molecules were removed from the structure. The carboxy-terminal four residues of the C subunit (Ala-Ala-Ala-Lys) are disordered in the crystal structure and are not included in these calculations. The isoprenoid tail of the ubiquinone-2 molecule was modified by applying the twofold symmetry operator between L and M subunits (Deisenhofer et al., 1995) to the tail of  $Q_A$ . Subsequent minimization of only the isoprenoid tail yielded a ubiquinone-7 model (UQ7) with headgroup coordinates identical to those determined for ubiquinone-2.

### Calculation of electrostatic energies

The analysis presented here assumes that the difference between the free energies of ionization of side chains in solution and within the protein is due solely to electrostatic free energy terms. For the calculation of electrostatic energies, several simplifying assumptions are made about the structure of the protein in different ionization states (Yang et al., 1993; Beroza et al., 1995). Thus, the x-ray structure is used for all protonation and redox states of the protein without modification of either heavy atom or nondissociatable proton positions. The effect of motions of the protein and solvent on changes in charge state is approximated by the response of a dielectric continuum.

The program DelPhi (Gilson et al., 1987; Sharp and Honig, 1990; Nicholls and Honig, 1991) was used to solve the Poisson equation to obtain the electrostatic potential in and around the RC, given a distribution of charges within the dielectric boundary of the protein (Gunner and Honig, 1991). A dielectric constant of 4 was assigned to the protein interior and 80

was used for water (Gilson and Honig, 1986). The use of a protein dielectric constant of 4 assumes that charges not only polarize electrons in the protein ( $\epsilon = 2$ ) but also cause some rearrangement of protein dipoles (Gilson and Honig, 1986). A dielectric constant of 4 has been used previously in the work of Beroza et al. (1995) and Gunner and Honig (1991, 1992). Gunner and Honig (1991) found that the calculation of electrochemical midpoint potentials of the four cytochrome hemes in the C subunit of *Rp. viridis* provided closer correspondence with the experimental data when  $\epsilon = 4$  than with  $\epsilon = 2$  or  $\epsilon = 6$ . Similar results were obtained by Beroza (1993). Antosiewicz et al. (1994) have suggested that  $\epsilon$  values as large as 20 improve the overall agreement with the experimental data for small soluble proteins such as lysozyme. The use of  $\epsilon = 4$  in this work is consistent with, and therefore allows comparison to, earlier calculations on RCs. A probe sphere radius (Richards, 1977; Connolly, 1983) of 1.4 Å was used to define the dielectric boundary between solvent and solute. The atomic van der Waals radii used were taken from Yang et al. (1993). No membrane was included in the calculations. Recent electrostatic calculations on the membrane protein bacteriorhodopsin with (Bashford and Gerwert, 1992) and without (Sampogna and Honig, 1994) a membrane model yielded basically the same results, so that the omission of a model membrane in this study is not likely to affect the general results. In addition, as will be discussed below, almost all of the residues of interest are located outside of the membrane in the cytoplasmic region of the protein complex.

The charge distributions on the amino acid side chains were taken from the CHARMM charge set (Brooks et al., 1983) as described by Gunner and Honig (1992). The charge distribution of the cofactors was adapted from Treutlein et al. (1992, cf. Table 1). The neutral quinone has a charge of +0.5 on the carbonyl carbon atoms and -0.5 on the carbonyl oxygen atoms. For the singly reduced quinone these values were 0.0 and -0.5; for the doubly reduced quinone they were 0.0 and -1.0, respectively (cf. Table 1). Neither  $Q_A$  nor  $Q_B$  was considered protonatable. Because the (singly reduced) unprotonated semiquinone  $Q_A^-$  or  $Q_B^-$  is stable and unprotonated over a wide pH range (Wraight, 1982), protonation of the quinone is only relevant for the transfer of the second electron to  $Q_B$ . The residues Arg, Asp, Cys, Glu, His, Lys, Tyr, the heme propionates, the chain termini, and the cofactors were treated as ionizable residues. All other residues were assumed to have no net charge. The histidine ligands of the nonheme iron, the bacteriochlorophylls, and the hemes (13 of the 29 His residues) were also assumed to remain neutral, as were the eight Cys residues involved in thioether bonds to the cytochrome heme groups; the N-terminal Cys of the C subunit, which is covalently bound via a thioether bond to a diacylglycerol (Weyer et al., 1987); and Cys L122, which is membrane-exposed and located in the middle part of transmembrane helix C (Deisenhofer and Michel, 1989). Ser L223 has been proposed to form a transiently protonated state, Ser L223-OH<sub>2</sub><sup>+</sup>, which could serve as a proton donor to the doubly reduced  $Q_B$  (Okamura and Feher, 1992). Ser L223 was therefore considered to be protonatable, with an estimated pK<sub>sol</sub> of -1.7 (Cometta-Morini et al., 1993), in a separate series of calculations.

Water molecules are not explicitly included in the calculations. The screening of charges by the external, solvent water is accounted for by the external dielectric constant of 80. Crystallographic, buried water molecules behave more like dipolar protein side chains than like a dielectric continuum. However, explicit inclusion of buried water molecules is difficult, because the water hydrogen atom positions are not unique. Protonation and deprotonation of neighboring amino acids will change the orientation of the water hydrogen atoms to stabilize both protonation states of a residue (Yang et al., 1993). Calculations that use only one water orientation optimized for a single ionization state can therefore introduce larger errors than if the charges on the water dipole are simply ignored (M. R. Gunner, unpublished observations). Without explicit water molecules, some stabilization of nearby polar or ionized residues is implicitly included by DelPhi, which puts a high dielectric constant in any cavities large enough to accommodate a water molecule.

DelPhi uses a grid-based, finite-difference method to solve Poisson's equation. A technique called focusing ensures adequate resolution in a protein as large as the *Rp. viridis* RC. A series of focusing calculations were made, centered on each site of interest (Gilson et al., 1987). All

**TABLE 1** Charges for nonstandard groups treated as ionizables in the calculations

Residue/cofactor		Neutral state	Ionized state
Chain termini			
Ctr	C	0.14	0.14
	OT1	-0.07	-0.57
	OT2	-0.07	-0.57
Ntr	CA	0.25	0.25
	N	-0.30	-0.30
	HT1	0.02	0.35
	HT2	0.02	0.35
	HT3	0.01	0.35
Heme propionates			
Pra	CBA/CBD	-0.16	-0.16
Prd	CGA/CGD	0.36	0.36
	O1A/O1D	-0.10	-0.60
	O2A/O2D	-0.10	-0.60
Bacteriochlorophylls/bacteriopheophytins			
Bcl	CAB	0.42	
Bph	CBB	0.10	
	OB <sub>B</sub>	-0.52	
	CAD	0.50	
	OBD	-0.50	
	CGD/CGA	0.55	
	O1D/O1A	-0.55	
	O2D/O2A	-0.45	
	CED/CP1	0.45	
Quinones			
	Q <sub>A</sub> /Q <sub>B</sub>	(Q <sub>A/B</sub> <sup>-</sup> )	(Q <sub>B</sub> <sup>2-</sup> )
O1	-0.50	-0.50	-1.00
C1	0.50	0.00	0.00
O4	-0.50	-0.50	-1.00
C4	0.50	0.00	0.00
C5	-0.10	=	=
CM5	0.10	=	=
C6	-0.10	=	=
UQ	C2/C3	0.05	=
UQ	O2/O3	-0.50	=
UQ	CM2/CM3	0.50	=
MQ	C2	-0.10	=
MQ	C3	-0.10	=
MQ	C3A	0.1	=
MQ	C3D	0.1	=
MQ	C7	0.1	=
Ser L223			
	HG1	0.4	0.4
	HG2	0.0	0.4
	OG	-0.65	-0.05
	CB	0.25	0.25

=, no change in the ionized state compared to the neutral state.

reported values are the result of a series of four calculations, with a final grid spacing of 0.59 Å/grid. Under these conditions, the calculated energy of interaction varies with position in the grid by less than 1%.

The electrostatic contributions of the free energy of a charge in the protein are separated into three energies, the reaction field energy ( $\Delta G_{rxn}$ ), the pH-independent interaction energy with partial charges on the protein backbone and polar side chains ( $\Delta G_{pol}$ ), and the pH (and redox state)-dependent interaction energy with other ionizable residues ( $\Delta G_{crg}$ ) (Gunner and Honig, 1992). The reaction field energy (or Born energy or solvation energy) is the result of the polarization of electrons and dipoles in the media that stabilizes a charge. When an ionizable group is transferred from

water to the low-dielectric environment of a protein, the loss of reaction field energy is referred to as the desolvation penalty ( $\Delta\Delta G_{rxn}$ ). This shifts ( $\Delta pK_{desolv}$ ) the ionization equilibrium toward the neutral form. However, interactions with specific polar and charged groups in the protein can compensate for the loss of reaction field energy to stabilize the ionized form of the residue. The groups in the protein are separated into sites whose charge or dipoles are always present and those groups whose charge state is the subject of these calculations. The former are referred to as pH-independent polar interactions and occur predominantly with the protein backbone and polar side chains. Their influence on the free energy is termed  $\Delta G_{pol}$ , which gives rise to  $\Delta pK_{pol}$ . The pH-independent contributions can be combined with the pK of this type of residue in solution ( $pK_{sol}$ ) to yield an "intrinsic pK" ( $pK_{int}$ ; Tanford and Kirkwood, 1957). The  $pK_{int}$  is defined as the  $pK_a$  that a titrating group in the protein would have if all other groups were in their neutral protonation states. Thus,

$$pK_{int} = pK_{sol} - c_a(\Delta pK_{desolv} + \Delta pK_{pol}), \quad (1)$$

where  $c_a$  is -1 if the site is an acid and +1 for a base. The pH- and redox-dependent charge-charge interactions with other ionizable residues change the free energy of ionization by  $\Delta G_{crg}$  if and when these sites are ionized.

### Calculation of amino acid titration by Monte Carlo sampling

For an ensemble of molecules of a protein with  $N$  titrating sites, there are  $2^N$  protonation states. Each protonation state of each protein molecule is defined by a vector of dimension  $N$ ,  $\mathbf{x} = (x_1, x_2, \dots, x^N)$ , where  $x_i$  is the protonation state of site  $i$ , specifying the number of protons bound (either 0 or 1). The free energy  $G(\mathbf{x})$  of the protonation state  $\mathbf{x}$  is given by (Yang et al., 1993)

$$G(\mathbf{x}) = \sum_{i=1}^N \delta_i(-kT \cdot \ln 10)(pK_{int,i} - pH) + 0.5 \sum_{i,j=1, j \neq i}^N \delta_i \delta_j \cdot \Delta G_{crg}(i,j), \quad (2)$$

where  $pK_{int,i}$  is the intrinsic  $pK_a$  of site  $i$ , the delta function  $\delta$  is 1 for an ionized residue and 0 for a neutral residue,  $k$  is Boltzmann's constant,  $T$  is the temperature, and  $\Delta G_{crg}(i,j)$  is the interaction energy between ionizable residues  $i$  and  $j$  when both are charged. Formally, the average protonation of a site in the ensemble of proteins  $\langle x_i \rangle$  is found by determining the statistical average (Boltzmann weighted sum) of all  $2^N$  protonation states of the protein complex:

$$\langle x_i \rangle = \frac{\sum_{\{x\}} x_i e^{-G(x)/kT}}{Z}, \quad (3)$$

where the sum is over all possible protonation states and  $Z$  is the partition function ( $Z = \sum_{\{x\}} e^{-G(x)/kT}$ ). However, use of Eq. 3 to determine  $\langle x \rangle$  is only practicable for small proteins (Bashford and Karplus, 1990). For proteins with more than 25 titrating sites, the time required to compute the free energy of every state becomes prohibitive (Beroza et al., 1991). Instead, it has been demonstrated that Monte Carlo sampling of protonation states yields reliable titration curves, even for very large proteins with strongly interacting sites (Beroza et al., 1991). Previous calculations on RCs have used Monte Carlo sampling to determine the average protonation state of each protonatable residue (Beroza et al., 1995; Gunner and Honig, 1992).

The average ionization of each site is the average of  $1.6 \cdot 10^6$  Monte Carlo sampled steps after 200,000 preequilibration steps. This provides a

**TABLE 2** The Q<sub>B</sub> cluster of the photosynthetic RC from *Rp. viridis*

pH-dependent charge-charge interaction energies ( $\Delta G_{\text{crg}}$  in  $\Delta pK$  units) of the ionizable amino acid residues of the  $Q_B$  cluster. To facilitate the identification of strong interactions, values  $\geq 2 \Delta pK$  units are highlighted (except for those with the pH-independent charges of  $\text{FeQ}^{2+}$  and its ligand Glu M232<sup>-</sup>). The information in the symmetric matrix is duplicated on both sides of the diagonal to facilitate the identification of all strong interactions associated with an individual residue. The division of residues between the  $Q_B$  cluster (this table) and the  $Q_A$  cluster (cf. Table 3) was not only based on direct couplings to the quinones alone. In some borderline cases, the stronger interactions with assigned members of the clusters were used as assignment criteria. Residues marked with a # are also listed in other tables as points of reference.

precision of  $\pm 2\%$  for the fractional protonation values of titrating residues. For the pH region between pH 5 and 11.5,  $3.2 \cdot 10^6$  Monte Carlo steps after  $1.6 \cdot 10^6$  preequilibration steps were employed. The longer computations provide a precision of  $\pm 1\%$ , as judged by selected runs of 80 cycles of 200,000 Monte Carlo steps. The Monte Carlo algorithm incorporates internal proton transfer by allowing two sites that are strongly interacting ( $|\Delta G_{\text{crg}}| > 2 \Delta pK$  units, i.e., 2.76 kcal/mol) to change state in a single Monte Carlo step 50% of the time, as suggested by Beroza et al. (1991).

In a complex group of interacting acids and bases, the titration of a residue may not be uniquely described by a single number in the form of a  $pK_a$  value. The  $pK'_a$  of a residue  $i$  will be defined as the pH value at which the average protonation  $\langle x_i \rangle$  is 0.5. As will become apparent below and has been shown by others previously (Bashford and Gerwert, 1992; Gunner and Honig, 1992; Beroza et al., 1995), the resulting titration curves are often quite different from classical (Henderson-Hasselbalch) single-site titration curves (cf. Figs. 3 and 4). Thus some residues have an average protonation of 0.5 over a range of pH values, as in a dicarboxylic acid, or display even more complex titration behavior (Sudmeier and Reilly, 1964), so that  $pK'_a$  may not be uniquely defined. However, for most residues, the  $pK'_a$  will provide a reasonable guide to the protonation state of this residue at a given pH value.

## **Calculation of proton uptake associated with the reduction of the quinones**

Calculation of proton uptake resulting from reduction of one or both of the quinones is accomplished by a separate calculation of the average site protonation for each of the redox states considered (cf. Fig. 1). Net proton uptake or release is obtained from the difference in average, summed protonation of all of the acids and bases in the RC (cf. Fig. 9 below). The role of individual sites is determined by subtraction of the average site protonation in the original state from that in the final redox state (cf. Fig. 4, below).

## RESULTS

## Identification of clusters of interacting residues

The calculations on the *Rp. viridis* RCs consider 288 protonatable residues. These include 64 Arg, 34 Lys, 16 nonligated His, 9 protonatable Cys, 47 Asp, 52 Glu, 52 Tyr, 8 propionates, 3 N-termini, and 3 C-termini. In addition, Ser L223 is included as an additional protona-

b) Contributions of loss of reaction field energy ( $\Delta\Delta G_{rxn}$ ) and pH-independent polar interactions ( $\Delta G_{pol}$ ) to the intrinsic pK ( $pK_{int}$ ) of the amino acid residues of the photosynthetic RC from *Rp. viridis*. Solution pK ( $pK_{sol}$ ) values: 12.5 (Arg), 3.9 (Asp), 4.3 (Glu), 6.5 (His), 10.8 (Lys), 8.0 (Ntr), 3.8 (Pra, Prd), -1.7 (Ser L223). Solution solvation energy (in  $\Delta pK$  units): -9.8 (Arg), -11.3 (Asp), -9.8 (Glu), -12.4 (His), -12.6 (Lys), -12.7 (Ntr), -14.0 (Pra, Prd), -12.4 (Ser L223).

$z$  coord. =  $z$  coordinate (in Å) after aligning the RC along the  $z$  axis (running perpendicular to the membrane) with the nonheme iron at the origin and the special pair of Mg atoms with  $z$  coord. = 27.7. The minimum  $z$  coordinate is -34.3 (Ala H191), the maximum is 98.5 (Gln C54);  $z$  coordinates for the Q<sub>B</sub> carbonyls are 0.6 (distal) and 2.1 (proximal).  $z$  coordinates are quoted for the following atoms of the respective residues: C $\zeta$  (Arg), C $\gamma$  (Asp), C $\delta$  (Glu), H $\beta$ 1 (His), C $\epsilon$  (Cys), N (Ntr), O4 (MQ7, UQ7); values between 0 and 27, thought to represent the hydrophobic region of the membrane bilayer, are highlighted.  $\Delta\Delta G_{rxn}$  = desolvation penalty (in ΔpK units); values > 5.0 are highlighted.  $\Delta G_{pol}$  = polar interaction energy (in ΔpK units); values > 5.0 are highlighted. pK<sub>int</sub> = intrinsic pK, see text for details; acidic residues with pK<sub>int</sub> < pK<sub>sol</sub> are highlighted.

table site in a second series of calculations. Groups of residues can be identified with ionization states that are interdependent because of the large electrostatic interaction energy between the sites when they are ionized. These will be referred to as clusters. Given a threshold criterion that charge-charge interactions change the  $pK$  of a residue by 2 pH units, a cluster of 47 titrating residues is identified that are directly or indirectly (i.e., via other titrating residues) coupled to  $Q_A$  and  $Q_B$ . Tyr and Cys residues are omitted from these clusters because all Tyr and Cys that are considered to be titratable (cf. Materials and Methods) are found to be neutral in all redox states of the protein at all pH values. The clusters can be subdivided into a group of 23 residues more strongly coupled to the ionization state of  $Q_B$  (the  $Q_B$  cluster; cf. Table 2), and another 24, which are more strongly coupled to  $Q_A$  (the  $Q_A$  cluster; cf. Table 3). The two clusters are linked via Glu M232, Asp H236, and Asp M238. Furthermore, the divalent cationic charge on the nonheme iron (FeQ) influences all residues near the quinones. Additional sites are found that change their ionization state in response to changes in the redox state of the quinones but have interactions smaller than the 2  $\Delta pK$  unit limit with the  $Q_A$  and  $Q_B$  clusters. These will be seen to lie in two regions, either on the cytoplasmic or on the periplasmic side of the protein complex. These cytoplasmic residues will be referred to as "marginal cytoplasmic sites" (cf. Table 4), and the periplasmic sites will be termed "isolated" (cf. Table 5). The rationale for this nomenclature will be discussed below.

# CONTRIBUTION OF $\Delta G_{rxn}$ AND $\Delta G_{pol}$ TO THE IONIZATION OF THE ACIDS AND BASES IN THE $Q_A$ AND $Q_B$ CLUSTERS

Table 2 contains the cluster of residues strongly coupled to the redox state of  $Q_B$ , Table 3 the sites coupled to  $Q_A$ , Table 4 the marginal cytoplasmic residues, and Table 5 the isolated periplasmic sites. Each of these four groups of residues differs in its reaction field energy ( $\Delta\Delta G_{rxn}$ ) and interactions with polar groups ( $\Delta G_{pol}$ ). We will first focus on the  $Q_B$  cluster. Desolvation penalties for sites in the  $Q_B$  cluster are sufficient to shift pK values by as much as 10 pH units relative to  $pK_{sol}$  in the absence of compensating polar interactions (Table 2b). As expected, more deeply buried residues have larger desolvation penalties. Deviations are found for residues such as Asp M230 (12.0 Å from the cytoplasmic surface) and Glu H177 (10.3 Å from the cytoplasmic surface) that are near cavities that have a radius of  $\geq 1.4$  Å and are therefore treated as having a dielectric constant of 80 by DelPhi. Also listed in Tables 2b and 3b are the coordinates along the membrane normal. Glu L104 is the only residue in the two tables that would be inside the low-dielectric region of the membrane. Despite the absence of a membrane model, this residue will be shown below to be neutral throughout the calculations. Thus, behavior of the

TABLE 3 The Q<sub>A</sub> cluster

Cf. footnote of Table 2 for details

residues of interest in this work are not expected to be modified significantly by the omission of a membrane in the calculations.

When the residues in the Q<sub>B</sub> cluster (Table 2) are ionized, their net interactions with polar groups in the protein are often substantial. These charge-dipole interactions can modify site pK values by as much as 15.4 pH units (e.g., Asp

**TABLE 4** The cytoplasmic “marginal” sites

#	Gcg	Arg	Arg	Asp	Glu	Glu	Glu	Glu	Lys	MQ7	UQ7	#
	(Δ pK)	M28	M130	M134	L218	M22	H45	L1	H234	M31	QA	QB
a)		+ +			-		-	+	-	+	-	-
Arg	N28	+	@ @	1.0	5.1	-11.4	-0.4				-0.1	-0.5
Arg	M130	+	@ @	1.8	-2.3	-0.2				-0.1	-0.6	-1.2
Arg	M134	+	@ @		7.6	-0.6				-0.1	-0.5	-1.1
Asp	L218	-			@ @	0.4				0.2	1.0	2.0
Glu	M22	-				@ @				0.1	0.2	0.3
Glu	H45	-								0.2	0.1	0.1
Ntr	L1	+								-0.3	-0.1	-0.2
Glu	H97	-								0.2	0.1	0.1
Glu	H216	-								0.1	0.1	0.1
Glu	H234	-								0.2	0.1	0.3
Lys	M31	+								0.2	0.1	0.3
#	MQ7	QA	-							-0.1	-0.2	-0.3
#	UQ7	QB	-							0.1	1.1	2.3
										@ @	@ @	@ @
b)	$\Delta$ Gcg (max.) with cluster member	coord.	(A)	-5.6	5.2	-2.0	-7.7	-7.6	-6.8	-4.3	-24.5	-25.0
											-1.6	1.4 2.1
$\Delta\Delta$ Gcxn	( $\Delta$ pK)	5.6	4.9	6.7	8.8	0.4	0.0	4.8	1.6	0.0	5.0	0.5
$\Delta$ Gpol	( $\Delta$ pK)	-0.5	-6.9	0.8	-1.1	0.6	0.5	-2.1	0.1	0.0	-6.3	0.9
pK (int)		7.4	14.5	5.0	11.7	5.2	4.8	5.3	5.9	4.3	3.0	9.4
pK (a)		-	-	10.5	-	3.5	-	7.0	3.6	4.0	-4	10.1

Cf. caption of Table 2 for details. Additional entries:  $\Delta G_{\text{crg}}$  (max.) with cluster member (in  $\Delta pK$  units) = maximum  $\Delta G_{\text{crg}}$  for the interaction with members of the  $Q_A$  or  $Q_B$  clusters.  $pK_a'$  = pH value for 50% protonation as defined in the text.

The cytoplasmic "marginal" sites are highlighted in boldface. Additional residues in plain print interact strongly with the members of this group. In the case of Arg M134, it is Asp L218 which provides the strongest interaction to a member of the QB cluster. Glu H216, Glu H234, and Lys M31 are isolated sites with no strong interactions with any other ionizable residue in the protein.

H174). With the exception of the nonheme iron ligand Glu M232, all acidic residues listed in Table 2 are stabilized by interactions with polar sites. Thus, polar sites generate a region of predominantly positive potential in the region of the Q<sub>B</sub> cluster. This favors ionization of acids and destabilizes ionization of the bases. For 9 of the 12 acidic residues, the pK<sub>in</sub> is lower than the pK<sub>sol</sub>. Thus, for these residues interactions with specific, polar sites in the protein more than compensate for the loss of the stabilization of the charge by water ( $\Delta\Delta G_{rxn}$ ). However, ionization of the basic

residues is destabilized by both the loss of reaction field energy and by interactions with the polar sites. The region of positive potential results largely from the orientation of the amide dipoles of the RC polypeptide backbone (cf. Fig. 2), as was previously observed for the *Rb. sphaeroides* RC by Gunner and Honig (1992) and Beroza et al. (1995). This dipole field is not uniform. Thus, permanent dipoles stabilize ionization of Glu H177 by  $-9.1 \Delta pK$  units and Asp M43 by only  $-2.7 \Delta pK$  units. The two acidic groups are only  $6.4 \text{ \AA}$  apart. Ionization of Glu H177 is favored by the five peptide bond interactions with a magnitude of greater than  $0.43 \Delta pK$  units. These are from L225 to L227 at the beginning of the transmembrane E helix and M232 and M233 at the beginning of a short helical segment. Conversely for Asp M43, of the five peptide bond interactions above the same threshold, only M44 stabilizes the charge. Interactions with H177 and H178, which are in a tight turn, and L223-L224, in a loop just before transmembrane helix E, destabilize the negative charge. These ten amide dipoles account for  $4.3 \Delta pK$  units of the  $6.4 \Delta pK$  unit net difference in the polar energy interactions of Glu H177 and Asp M43.

The aforementioned extreme charge-dipole interaction energy calculated for Asp H174 is also predominantly due to peptide bond dipoles, which contribute +580 mV to the electrostatic potential at the Cy position of Asp H174, although there is a substantial contribution from the side chain of Arg H181, which contributes 2.3  $\Delta pK$  units, even in its neutral dipolar form. The residue Asp H174 is located at the end of a  $\beta$ -strand, and it is the peptide bonds of the following tight turn (H176–H178) which make the largest contribution (5.5  $\Delta pK$  units in total), but many other peptide dipoles contribute to the remainder of the charge-dipole interaction energy of 15.4  $\Delta pK$  units toward stabilizing the charge on this residue.

The environment of the residues in the Q<sub>A</sub> cluster and the isolated residues coupled to quinone ionization is different from that found for the Q<sub>B</sub> cluster. Although there are individual sites with  $\Delta\Delta G_{rxn}$  sufficient to shift the pK by 9 pH units, there are also residues in Tables 3 and 4 that have much smaller  $\Delta\Delta G_{rxn}$ . In addition, the influence of the polar groups is smaller and less uniform. Thus, ionization of both acids and bases in Tables 3 and 4 is stabilized by interactions with polar groups. However, no group in the Q<sub>A</sub> cluster or the marginal cytoplasmic sites experiences sufficient  $\Delta G_{pol}$  to compensate for the loss in reaction field energy. Therefore, in the absence of interactions with other RC acids and bases, all of these sites would be more difficult to ionize *in situ* than they would be in solution.

## **INTERACTIONS AMONG THE IONIZABLE RESIDUES IN THE Q<sub>A</sub> AND Q<sub>B</sub> CLUSTERS**

Inspection of the interactions within the  $Q_B$  cluster shows that there is a hierarchy of interactions. Thus, there are several groups of sites that are very tightly coupled, with each connected to other sites in the cluster by weaker

**TABLE 5** The periplasmic “isolated” sites

Residue	Asp M182	Glu C79	Glu C254	Glu M76	His M162	Ntr C1	Pra 1a
a)							
$\Delta G_{\text{crg}}$ ( $\Delta pK$ units)							
# MQ7 Q <sub>A</sub>	0.3	<0.1	0.2	0.1	-0.3	-0.2	<0.1
# UQ7 Q <sub>B</sub>	0.4	<0.1	0.2	0.2	-0.3	-0.3	<0.1
$\Delta G_{\text{crg}}$ (max.)	0.4	>-0.1	0.2	0.2	-0.3	0.3	>-0.1
with cluster member	Q <sub>B</sub>	Arg L231	Q <sub>A</sub>	Q <sub>B</sub>	Q <sub>B</sub>	Arg L231	Arg L231
b)							
z coord.	36.3	72.2	43.2	37.0	29.4	32.8	88.3
$\Delta \Delta G_{\text{rxn}}$ ( $\Delta pK$ )	9.3	3.0	7.6	5.6	10.5	0.7	7.9
$\Delta G_{\text{pol}}$ ( $\Delta pK$ )	-6.6	0.1	-6.2	-1.3	-4.3	0.9	-6.5
pK <sub>int</sub>	6.6	7.4	5.8	8.6	0.3	6.5	5.3
pK' <sub>a</sub> (DQ <sub>A</sub> Q <sub>B</sub> )	6.2	7.1	7.4	9.6	4.4	6.9	6.3

Periplasmic residues calculated to exhibit protonation differences upon changes in the quinone redox states (cf. footnotes of Tables 2 and 4 for details).

interactions (cf. Table 2a). Of the ionizable residues, only Glu L212, which is located 6.6 Å away from the proximal carbonyl oxygen of Q<sub>B</sub>, has a free energy of interaction with Q<sub>B</sub><sup>-</sup> of more than 2 ΔpK units. Glu L212 then interacts strongly with the nine residues Glu L210, Asp H174, Arg M231, Asp H125, Lys H133, Arg H181, Asp M230, Glu H177, and Glu M234. These residues, in turn, interact strongly with other residues. A number of other residues that modify the electrostatic potential in the vicinity of Q<sub>B</sub> and the Q<sub>B</sub> cluster without being able to play a role in coupling proton and electron transfer are also included in Table 2. Thus, the 2+ charge on the nonheme iron raises the potential throughout this region of the protein. Furthermore, its ligands Glu M232 and His L190 are coupled strongly to Q<sub>B</sub>, but the former is always ionized and the latter always neutral because of their interaction with the FeQ<sup>2+</sup>. The electrostatic interactions are twice as large for Q<sub>B</sub><sup>2-</sup> than Q<sub>B</sub><sup>-</sup>. This raises the number of ionizable residues interacting directly with the quinone by more than 2 ΔpK units from 1 to 9. Also included as a protonatable residue is Ser L223, which in its protonated form is a potential proton donor to the reduced Q<sub>B</sub>. This residue will be shown to be ionized only when Q<sub>B</sub> is doubly reduced.

A rough correlation is found between the reciprocals of the shortest distances between (de-)protonatable atoms and the charge-charge interaction energies (in Tables 2a–4a) of each pair of residues. However, there are deviations from a straight linear relationship that can be correlated with increasing solvent accessibility of the sites. For instance, most of the interactions with a magnitude of 2.3 ΔpK units are between sites approximately 10 Å apart (e.g., Glu L212-Arg M231, Glu L212-Asp H125) whereas the amino terminus of the M subunit (Ntr M1) and Arg M226 interact equally strongly, but are only 4.7 Å apart. The latter sites are much better solvated, which is reflected by low desolvation penalties (cf. Table 2b) leading to increased screening of the two interacting charges.

Q<sub>A</sub> is similar to Q<sub>B</sub> in that there are few sites that have strong direct interactions with the quinone. The nonheme

iron FeQ and its ligand Glu M232 have almost identical interactions with both quinones. Glu L104 and Asp H36 are the only protonatable residues strongly coupled to Q<sub>A</sub>. Glu L104 is deeply buried, and when it is protonated it can form a hydrogen bond to the ring V keto carbonyl group of φ<sub>A</sub> and so has a pK<sub>int</sub> of 16.2 (cf. Table 3). It is calculated to be neutral in all redox states at all pH values. Although Asp H36 has a pK<sub>int</sub> of 7.6, it is involved in a salt bridge with Arg H33. This effect alone shifts the pK<sub>a</sub> of this residue by -9.1 ΔpK units, causing both residues to be ionized throughout the calculations. Interactions just above the 2 ΔpK unit threshold provide extensions of the cluster from Asp H36 to Glu H35 and Glu M261, which, in turn, interact strongly with other residues (cf. Table 3).

The Q<sub>A</sub> and Q<sub>B</sub> clusters are the same size (24 and 23 residues, respectively). Each shows the quinone to be coupled to the cluster via a very small number of sites. However, there are a number of significant differences between the two clusters. The Q<sub>B</sub> cluster has 13 acidic residues and 10 basic residues, resulting in a surplus of three acidic residues. This imbalance is maintained in the center of the cluster, where Glu L212 interacts strongly with twice as many acidic as basic residues (vide supra). The average desolvation penalty in the Q<sub>B</sub> cluster is 6.6 ΔpK units. Without considering the interactions with the nonheme iron, the iron’s ligand Glu M232, or Q<sub>A</sub>, there are 87 charge-charge interactions with energies greater than 2 ΔpK units. In contrast, the 24 residues of the Q<sub>A</sub> cluster (10 acidic, 14 basic) are coupled by only 41 strong charge-charge interactions (cf. Table 3a) and experience an average desolvation penalty of 5.5 ΔpK units. In summary, the Q<sub>A</sub> cluster differs from the Q<sub>B</sub> cluster in four important characteristics. The Q<sub>A</sub> cluster has a surplus of basic residues, whereas the Q<sub>B</sub> cluster has a surplus of acidic residues; the Q<sub>A</sub> cluster has fewer and smaller charge-charge interactions within the cluster; its residues are more solvated; and, as discussed above, the dipolar groups stabilize negative charges less than in the Q<sub>B</sub> cluster.

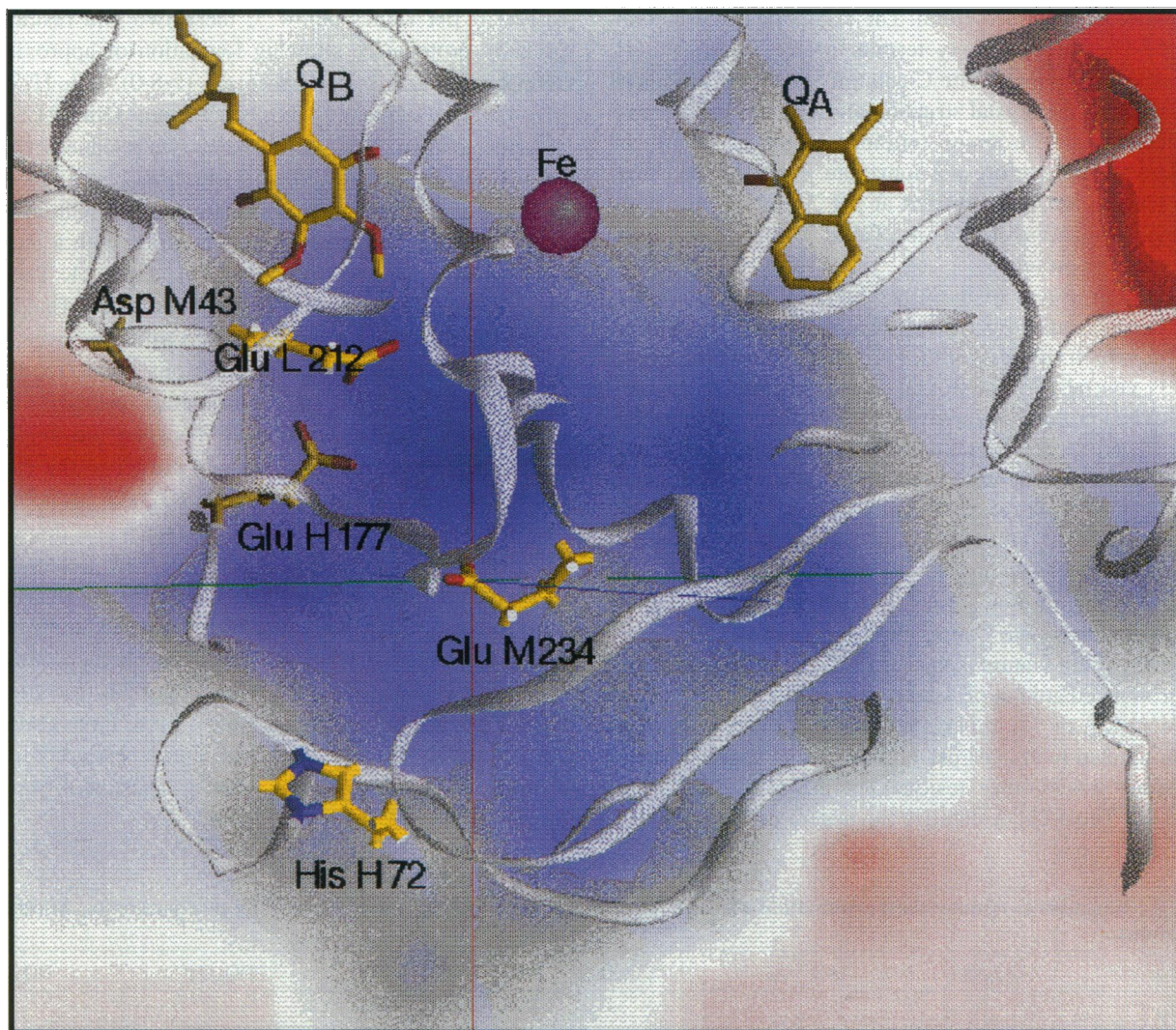


**FIGURE 2** Contribution of the polypeptide backbone to the electrostatic potential in the RC. Depicted is a slice plane parallel to the quinones and the nonheme iron running through the C $\delta$  of Glu M234. Largest magnitudes are +900 mV (blue) for Glu L210 NH and -1260 mV (red) for Glu H61 O. The largest side-chain magnitudes are +720 mV for Asp H174 O $\delta$  and -900 mV for Arg M245 NH1. The corresponding values for the depicted residues are +460 mV for Glu M234 C $\delta$ , +435 mV for Glu H177 C $\delta$ , +385 mV for Glu L212 C $\delta$ , and 0 mV for Asp M43 C $\gamma$ . This illustration was made with GRASP (Nicholls et al., 1991). An electronic version of this Figure can be viewed on the World Wide Web at [http://www.rzt.uni-frankfurt.de/~fx7005/BJ\\_B50863\\_figs.html](http://www.rzt.uni-frankfurt.de/~fx7005/BJ_B50863_figs.html).

The marginal cytoplasmic sites represent a diverse group. The four isolated cytoplasmic residues (Glu M22, Glu H97, Glu H216, and Lys M31) are virtually solvent-exposed, with an average desolvation penalty of 0.6  $\Delta pK$  units, and are electrostatically isolated. The other marginal cytoplasmic sites (Arg M134, amino terminus (Ntr) L1, and Glu H234) are part of several strongly coupled miniclusters that are coupled to residues of the Q<sub>A</sub> or Q<sub>B</sub> clusters by interactions below the 2  $\Delta pK$  unit threshold (cf. Table 4a). These three residues experience an average desolvation penalty of 5.5  $\Delta pK$  units. The isolated periplasmic sites are part of a single, large cluster of interacting residues around the primary donor D and within the C subunit. These residues are virtually isolated from Q<sub>A</sub>, Q<sub>B</sub>, and their associated clusters (cf. Table 5), but their pK<sub>a</sub> values are in the pH range of

interest, so even small changes in the electrostatic potential cause shifts in their protonation state.

## CALCULATION OF TITRATION CURVES BY MONTE CARLO SAMPLING

### Redox state DQ<sub>A</sub>Q<sub>B</sub>

In the ground state (DQ<sub>A</sub>Q<sub>B</sub>) the isoelectric point of the RC, i.e., the pH value at which the net charge is zero, is calculated to be 5.8, which is slightly lower than the value of 6.5 observed experimentally by Welte et al. (1983). At pH 7, all Arg, and all but one Asp, all but eight Glu, and all but two Lys residues as well as three propionates are calculated to be fully ionized, whereas all Tyr and all but one of the His

residues are found to be neutral. The exceptions are found in Table 6. The three carboxy termini of the L, M, and H subunits are all ionized. The C subunit carboxy terminus is not resolved in the crystal structure and was not included in the calculations. The amino terminus of the H subunit is formylated and therefore not ionizable. None of the other amino termini are fully ionized at pH 7. The groups with fractional ionization listed in Table 6 are distributed throughout the protein.

Despite the excess of basic residues, all residues in the  $Q_A$  cluster are ionized between pH 5.5 and 10.5, except for Lys H66, which titrates with a  $pK_a'$  of 9.1, and Glu L104, which is neutral. Within the  $Q_B$  cluster, residues are predominantly ionized between pH 5.0 and 10.5, despite the excess of acidic residues and high desolvation penalties. The exceptions are the amino terminus of the M subunit and His H72, which are predominantly neutral, and the three residues Glu L212, Glu H177, and Glu M234. These three form a strongly interacting unit that will be referred to as the Glu cluster. The titration curves for the three glutamic acids, as calculated by Monte Carlo sampling, are shown in Fig. 3. The most striking feature is that Glu L212 is calculated to be more protonated at high pH than at low pH values (Fig. 3 a). Despite a  $pK_{int}$  of 3.6, this residue appears to be more than 50% protonated to at least pH 11. The strong charge-charge interactions when other residues in the Glu cluster are ionized (cf. Table 2a) destabilize the negative charge on Glu

L212. At pH values below 7, these two Glu residues are partially protonated, allowing ionization of approximately 35% of Glu L212. At higher pH (>8.0), Glu H177 and M234 are predominantly ionized, whereas Glu L212 is now more protonated. None of the three Glu residues exhibits a typical Henderson-Hasselbalch titration curve. However, the sum of the fractional protonation of the Glu cluster is approximately described by such a curve, with a total protonation of 2 near pH 5, and of 1 near pH 11. The  $pK_a'$ ,  $pK_a''$ , and  $pK_a'''$  values of the Glu cluster are defined as the points of inflection in the calculated titration curve, corresponding to a summed fractional protonation of 0.5, 1.5, and 2.5, respectively. We shall concentrate primarily on the  $pK_a''$  values for the equilibrium between the singly and doubly protonated states of the Glu cluster in the different RC redox states. In the ground state ( $DQ_A Q_B$ ) it is 6.4. The  $pK_a''$  value, i.e., the equilibrium between the doubly and triply ionized states, is calculated to be much greater than 20 in the ground state because Glu L212 remains overwhelmingly neutral when the other two acids are ionized. The  $pK_a'''$  value (i.e., the equilibrium between the doubly and fully protonated states) is only important for the state  $DQAQ_B^{2-}$  (cf. below). In summary, these three glutamates act as a tightly coupled cluster of interdependently titrating residues within the larger  $Q_B$  cluster. These will be seen to function as a buffer for the  $Q_B$  site.

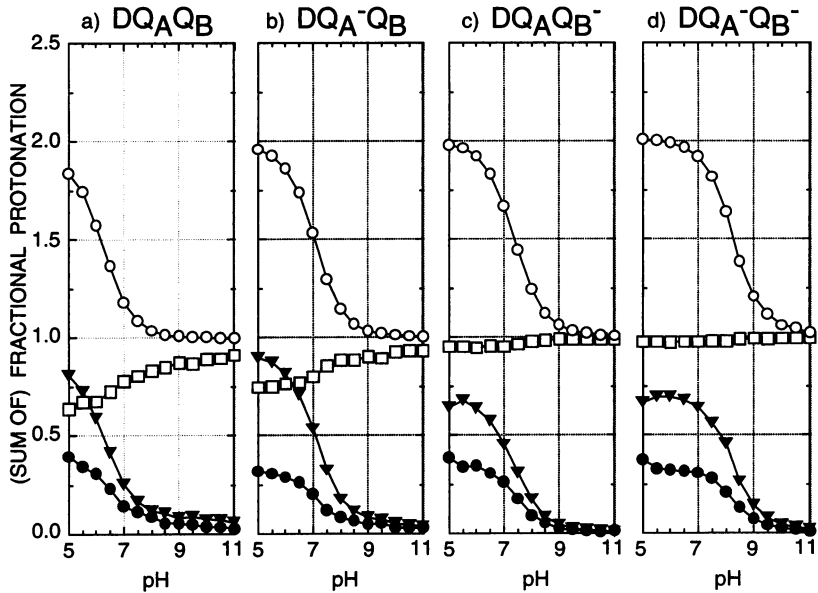
**TABLE 6** Residues in nonstandard protonation states at pH 7 in the state  $DQ_A Q_B$  and their average protonation  $\langle x_i \rangle$  in other redox states

Residue	$DQ_A Q_B$	$DQ_A^- Q_B$	$DQ_A Q_B^-$	$DQ_A^- Q_B^-$	$DQ_A Q_B^{2-}$	$DQ_A Q_B^{2-*}$
$Q_B$ cluster						
Glu H177	0.14	<b>0.20</b>	<b>0.26</b>	<b>0.31</b>	<b>0.98</b>	0.98
Glu L212	0.78	<b>0.80</b>	<b>0.95</b>	<b>0.98</b>	<b>1.00</b>	1.00
Glu M234	0.25	<b>0.53</b>	<b>0.45</b>	<b>0.64</b>	<b>0.73</b>	<b>0.48</b>
Ntr M1	0.00	0.01	0.01	0.01	0.01	0.01
$Q_A$ cluster						
Glu L104	1.00	1.00	1.00	1.00	1.00	1.00
Lys H66	0.98	0.99	0.98	<b>1.00</b>	1.00	1.00
Cytoplasmic						
Ntr L1	0.52	<b>0.66</b>	<b>0.54</b>	<b>0.68</b>	<b>0.65</b>	0.64
Lys H89	0.98	0.99	0.99	0.98	0.99	0.99
Periplasmic						
Asp M182	0.33	<b>0.35</b>	0.34	<b>0.39</b>	<b>0.51</b>	0.50
Glu C48	0.05	0.05	0.05	0.05	0.05	0.05
Glu C79	0.56	0.57	0.58	0.56	<b>0.62</b>	0.60
Glu C254	0.63	<b>0.65</b>	0.65	0.67	<b>0.69</b>	0.68
Glu M76	0.95	0.95	0.96	0.95	0.96	0.96
His M162	0.07	0.07	0.08	0.08	<b>0.11</b>	0.11
Ntr C1	0.48	0.49	<b>0.51</b>	<b>0.54</b>	<b>0.67</b>	<b>0.65</b>
Pra 1a	0.22	0.21	0.22	0.23	0.23	0.23
Prd 2d	1.00	1.00	1.00	1.00	1.00	1.00
Pra 3a	0.03	0.03	0.03	0.02	0.02	0.02
Pra 4a	0.91	0.91	0.91	0.92	0.92	0.92
Prd 4d	0.02	0.02	0.02	0.02	0.02	0.02

Bold numbers indicate changes greater than 0.01  $H^+$  compared to the redox state one column further left.

\*Only the last column refers to the calculations including Ser L223 as an ionizable, all other columns do not.

**FIGURE 3** Titration curves (i.e., (average) fractional protonation as a function of pH) as calculated from Monte Carlo sampling for the three residues Glu H177 (●), Glu L212 (□), and Glu M234 (▼) in the first four redox states highlighted in Fig. 1 and the sum of their fractional protonation (○ Glu cluster). Each of these titration curves is the result of 16 cycles of 200,000 Monte Carlo iterations. (a)  $DQ_A Q_B$ . (b)  $DQ_A^- Q_B$ . (c)  $DQ_A Q_B^-$ . (d)  $DQ_A^- Q_B^-$



### Proton uptake coupled to changes in the redox state of the quinones

Even though the exact assignment of partial ionization within the tightly coupled cluster is difficult to calculate owing to the interdependence of the ionization of sites, protonation changes are quoted to two significant figures after the decimal point. This is done because many sites are calculated to exhibit small changes in protonation, and the rounding error would be substantial if the second decimal were ignored. The work reported here does not consider redox states involving the oxidized primary donor  $D^+$  or oxidized cytochromes. Formation of  $D^+$  leads to proton efflux to the periplasm (calculated to involve particularly Asp M182 and Glu C254, two of the “isolated” periplasmic sites; Table 5). There are likely to be additional changes as the hemes in the C subunit are oxidized as  $D^+$  is reduced (Gao et al., 1990). Although the redox events near the periplasm modify the total proton uptake, this is calculated to have no influence on the protonation of the  $Q_B$  and  $Q_A$  clusters, which is the focus of the work reported here, so that these states are excluded from this study.

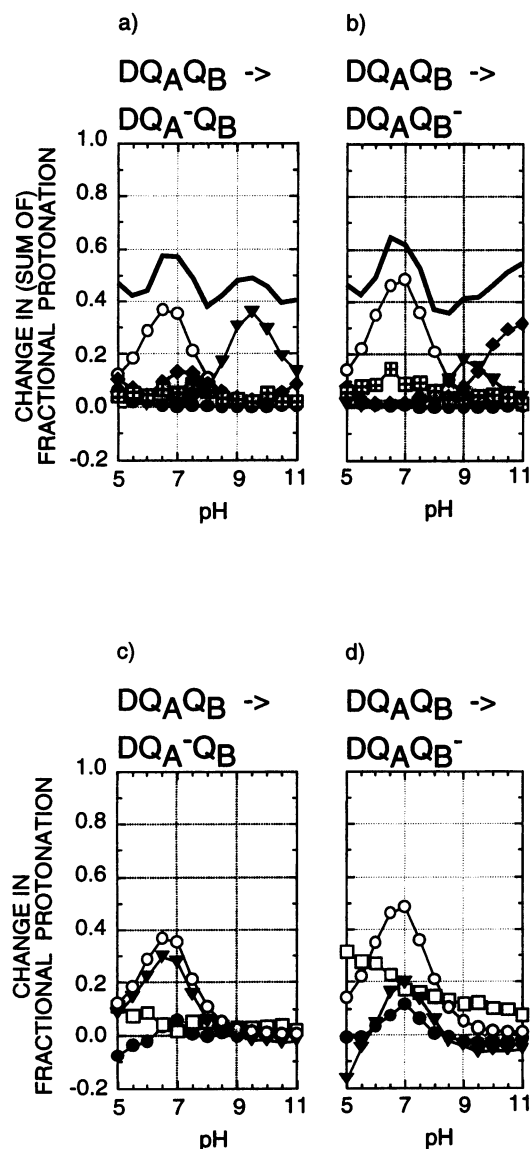
#### Redox state $DQ_A^- Q_B$ and the transition $DQ_A Q_B \rightarrow DQ_A^- Q_B$

Fig. 4 *a* shows the pH-dependent profiles of the change in protonation upon transfer of the first electron to  $Q_A$  ( $DQ_A Q_B \rightarrow DQ_A^- Q_B$ , step 1 in Fig. 1). This should correspond to the total proton uptake by the protein when the RC goes from the ground state to the  $DQ_A^-$  state. At pH 7.0, the net, average change for the entire protein complex is +0.57 protons per RC (see Table 6). This is predominantly due to nine sites that bind at least 0.01 H<sup>+</sup> per site and one periplasmic site that releases more than 0.01 proton per site (see Fig. 4, *c* and *a*). Despite the stronger interaction between the  $Q_A$  cluster and  $Q_A$ , the protonation of each site of

the  $Q_A$  cluster except for Lys H66 (+0.01 H<sup>+</sup>) is unaffected at neutral pH by the ionization state of  $Q_A$ . Rather, the bulk of the proton uptake on reduction of  $Q_A$  is in the  $Q_B$  cluster, with +0.35 H<sup>+</sup> localized in the Glu cluster. At pH 7 this is mostly due to protonation of Glu M234 (see Fig. 4 *c*). The reduction of  $Q_A$  shifts the pK<sub>a</sub>'' of the Glu cluster from 6.4 to 7.1 (Fig. 3 *b*). In addition, the marginal cytoplasmic site Ntr L1 binds on average +0.13 H<sup>+</sup>, whereas isolated periplasmic sites bind +0.06 H<sup>+</sup>.

Fig. 4 *a* shows that the stoichiometry of proton uptake after reduction of  $Q_A$  is remarkably independent of the pH, remaining between 0.4 and 0.6 H<sup>+</sup>/RC between pH 5 and 11. However, the sites that are responsible do change as the pH changes. Thus, proton uptake at higher pH is now due to charges in the  $Q_A$  cluster, predominantly Lys H66 (+0.36 H<sup>+</sup> at pH 9.5; cf. Fig. 4 *a*). Consequently, between pH 6.0 and pH 8.0, the  $Q_B$  cluster dominates the total calculated uptake of the protein, whereas between pH 8.0 and pH 10.5, residues in the  $Q_A$  cluster are more important. The effect of having such a large group of residues with interdependent ionization properties is that at different pH values, different residues change their ionization, but the net proton uptake is relatively constant.

In addition to the important role of the groups in the  $Q_A$  and  $Q_B$  clusters, the residues in Tables 4 and 5 are calculated to contribute to proton uptake after electron transfer. The change in ionization of these isolated sites is a consequence of the sensitivity of the protonation state to small changes in the electrostatic potential when the residue is near its pK. Thus, at the pK a 10-meV change in the free energy of ionization, corresponding to a shift of 0.17 ΔpK units, will change the average protonation by 0.1 proton. Although the contribution of the individual sites is small at neutral pH, they contribute 0.1 to 0.3 H<sup>+</sup> to the total protonation of protein over the entire pH range (cf. Figs. 5 *c*).



**FIGURE 4** Protonation differences for the transfer of the first electron. Symbols for *a* and *b*: —, change in the average net protonation of the whole RC excluding quinone cofactors, i.e., total calculated uptake; ○, summed contribution of the three Glu residues H177, L212, and M234 (Glu cluster); ●, difference between contribution of the  $Q_B$  cluster and that of the Glu cluster; ▼, the  $Q_A$  cluster; ♦, the “marginal cytoplasmic sites”; ■, the “isolated periplasmic sites.” The symbols for *c* and *d* are assigned to three residues Glu H177 (●), Glu L212 (□), and Glu M234 (▼) and to the sum of their fractional protonation (○ Glu cluster). (*a* and *c*)  $DQ_AQ_B \rightarrow DQ_A^-Q_B$  (i.e., step 1 in Fig. 1). (*b* and *d*)  $DQ_AQ_B \rightarrow DQ_AQ_B^-$

#### Redox state $DQ_AQ_B^-$ and the transition $DQ_AQ_B \rightarrow DQ_AQ_B^-$

Also displayed in Fig. 4 are the pH-dependent profiles of the change in protonation upon transfer of the first electron from the ground state to  $Q_B$  ( $DQ_AQ_B \rightarrow DQ_AQ_B^-$ ) for residues in the Glu cluster (cf. Fig. 4 *d*), for the identified clusters, and for the entire protein (excluding quinone cofactors; cf. Fig. 4 *b*). Substoichiometric proton uptake is observed with a maximum proton uptake of  $0.65 H^+$ . At pH

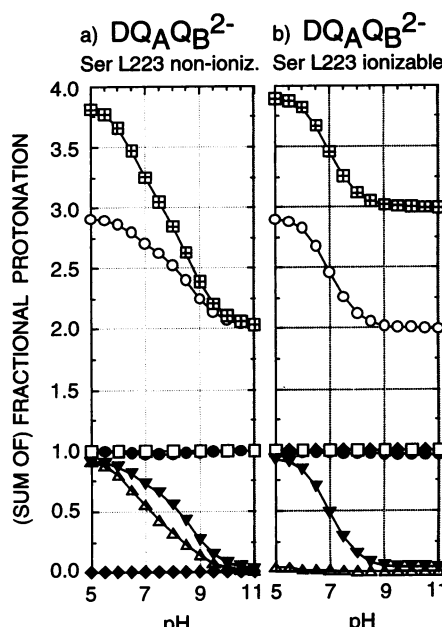


**FIGURE 5** Titration curves (i.e., fractional protonation as a function of pH) as calculated from Monte Carlo sampling for the five residues Asp M43 (△), Glu H177 (●), Glu L212 (□), Glu M234 (▼), and Ser L223 (♦) in the fifth redox state ( $DQ_AQ_B^{2-}$ ) highlighted in Fig. 1, and the sum of their fractional protonation (■). The summed fractional protonation of the three Glu residues is plotted separately (○ Glu cluster). Each of these titration curves is the result of 16 cycles of 200,000 Monte Carlo iterations. Not all symbols are shown for all calculated results, because of spatial overlaps. Calculations excluded (*a*) or included (*b*) Ser L223 as an ionizable residue. See text for details.

7.0, the net change for the entire protein complex is  $+0.62 H^+$  (see Table 6). The net uptake by the Glu cluster is  $0.49 H^+$ , which is approximately evenly divided among the three individual residues. In addition, there are small contributions by isolated periplasmic (e.g., Asp M182) and marginal cytoplasmic (e.g., Ntr L1) sites. Apart from these five residues, no protonation differences larger than  $0.01 H^+$  are observed at this pH value. The Glu cluster within the  $Q_B$  cluster dominates the calculated total uptake for the protein between pH 6 and 8.5. Thus, the peak in total proton uptake at pH 6.5 corresponds to the maximum for the cluster. The  $Q_A$  cluster makes its most significant contribution near pH 9. Above pH 9.5 the largest contribution is from Arg M134 ( $+0.29 H^+$  at pH 11) of the isolated cytoplasmic sites. The  $pK_a$  of the Glu cluster is increased from 6.4 to 7.4 as the reaction center goes from the ground  $DQ_AQ_B$  to the  $DQ_AQ_B^-$  state.

#### Redox state $DQ_A^-Q_B^-$ and the transition $DQ_AQ_B^- \rightarrow DQ_A^-Q_B^-$

Transfer of the second electron to  $Q_A$  yields the redox state  $DQ_A^-Q_B^-$ . Compared to the ground state  $DQ_AQ_B$ , net protonation at pH 7 is calculated to increase by  $+1.11 H^+$ , whereas  $+0.16 H^+$  is attributed to the marginal cytoplasmic

Ntr L1 (see Table 6). The net uptake of the Glu cluster is  $+0.74\text{ H}^+$ . An additional  $+0.02\text{ H}^+$  is provided by the  $\text{Q}_\text{A}$  cluster. The  $\text{pK}_\text{a}''$  of the Glu cluster is 8.3, 1.9 pH units higher than in the ground state (cf. Fig. 3 d).

#### *Redox state $\text{DQ}_\text{A}\text{Q}_\text{B}^{2-}$ and the transition $\text{DQ}_\text{A}\text{Q}_\text{B} \rightarrow \text{DQ}_\text{A}\text{Q}_\text{B}^{2-}$*

Formation of the  $\text{Q}_\text{A}^-$  or  $\text{Q}_\text{B}^-$  states yields substoichiometric proton uptake that is distributed among several residues. In contrast, the state  $\text{DQ}_\text{A}\text{Q}_\text{B}^{2-}$  creates large changes in the equilibrium ionization state of the protein (see Fig. 5 a and Table 6). Thus, the  $\text{pK}_\text{a}'''$  of the Glu cluster shifts from 7.4 in the state  $\text{DQ}_\text{A}\text{Q}_\text{B}^-$  to approximately 36, demonstrating the destabilization of the doubly ionized form of the cluster in the presence of  $\text{Q}_\text{B}^{2-}$ . In this state, the  $\text{pK}_\text{a}'''$  value of the Glu cluster, referring to the  $\text{pK}$  of the cluster for the binding of the third proton, was determined to be 8.4 (it is below 0 in all the other redox states). The  $\text{pK}_\text{a}$  of the nearby Asp M43 undergoes a shift of approximately 17 units upon formation of the state  $\text{DQ}_\text{A}\text{Q}_\text{B}^{2-}$  from much less than 0 to 7.7.

The net difference between the ground state  $\text{DQ}_\text{A}\text{Q}_\text{B}$  and the state  $\text{DQ}_\text{A}\text{Q}_\text{B}^{2-}$ , i.e., after the transfer of two electrons to  $\text{Q}_\text{B}$ , is shown below in Fig. 9 c. At pH 7, if the protein came into equilibrium without proton transfer to  $\text{Q}_\text{B}$ , the net change in protonation of the whole protein is calculated to be  $+0.20\text{ H}^+$ . Protonation changes greater than  $+0.20\text{ H}^+$  per site are restricted to the members of the Glu cluster, which binds an extra  $+1.52\text{ H}^+$ , and Asp M43, which binds on average  $0.55\text{ H}^+$  at pH 7. The contribution of the isolated sites is  $0.3\text{--}0.6\text{ H}^+$  up to pH 9 and increases to  $1.0\text{ H}^+$  at pH 11 ( $+0.7\text{ H}^+$  at pH 11 is accounted for by Arg M134). The summed contribution of the  $\text{Q}_\text{A}$  cluster and the  $\text{Q}_\text{B}$  dominates the total uptake of the protein in the pH range 6–10.5.

#### *Explicit inclusion of the protonation of Ser L223 in the redox state $\text{DQ}_\text{A}\text{Q}_\text{B}^{2-}$*

The presence of a doubly reduced  $\text{Q}_\text{B}$  appears to perturb the environment of the  $\text{Q}_\text{B}$  site so much that Ser-OH $_2^{2+}$  could become an accessible intermediate. When a protonatable Ser is included in the calculations with a  $\text{pK}_\text{sol}$  of  $-1.7$ , 2.97 protons are bound by the protein on the transition  $\text{DQ}_\text{A}\text{Q}_\text{B} \rightarrow \text{DQ}_\text{A}\text{Q}_\text{B}^{2-}$  at pH 7, with  $+0.67\text{ H}^+$  accounted for by isolated sites (see Table 6). The Glu cluster displays a net change in protonation of  $+1.26\text{ H}^+$  (see Table 6), and the calculated uptake for Ser L223 is  $+1.0\text{ H}^+$ .

## SUMMARY AND VISUALIZATION OF PROTONATION CHANGES IN TERMS OF ELECTROSTATIC POTENTIAL DIFFERENCES

The calculations reported here provide the change in electrostatic potential near the quinone as the protein goes through the cycle in Fig. 1. This change results from the added negative charges as each quinone is reduced in turn

and the induced shifts in residue protonation. The change in potential was obtained, given the charge on the quinone plus the calculated average protonation of each residue at pH 7 in each of the five important redox states. The resulting electrostatic potential differences are displayed as color-coded contour maps shown in Fig. 6. This enables the impact of the changes in protonation shown in the titration curves to be followed within the RC structure.

The primary impact of the reduction of  $\text{Q}_\text{A}$  is to make the vicinity of  $\text{Q}_\text{A}$  more negative (see Fig. 6 a). There is some compensating proton binding. However, at pH 7, the latter change is seen to occur predominantly in the vicinity of  $\text{Q}_\text{B}$ . This is due mostly to an increase in the average protonation of Glu M234 by  $+0.28\text{ H}^+$  and a small increase in protonation of Glu H177 ( $+0.06\text{ H}^+$ ). This proton uptake near  $\text{Q}_\text{B}$  on reduction of  $\text{Q}_\text{A}$  may be important for preparing the  $\text{Q}_\text{B}$  site to receive an electron from  $\text{Q}_\text{A}$ .

When the electron is transferred from  $\text{Q}_\text{A}$  to  $\text{Q}_\text{B}$  at pH 7, the primary change is that  $\text{Q}_\text{A}$  is more positive and  $\text{Q}_\text{B}$  is more negative (see Fig. 6 b). In response, the  $\text{Q}_\text{B}$  cluster binds an additional  $+0.14\text{ H}^+$ . This involves protonation of Glu H177 ( $+0.06\text{ H}^+$ ) and Glu L212 ( $+0.15\text{ H}^+$ ), partially at the expense of deprotonation of Glu M234 ( $-0.08\text{ H}^+$ ). When visualized in terms of molecular geometry (cf. Fig. 6 b), this effect can be understood as a substoichiometric proton transfer from Glu M234 (which is  $13.8\text{ \AA}$  from  $\text{Q}_\text{B}$ ) to Glu H177 ( $8.1\text{ \AA}$  from  $\text{Q}_\text{B}$ ) and Glu L212 ( $6.6\text{ \AA}$  from  $\text{Q}_\text{B}$ ) to achieve better charge compensation for the negative charge arriving on  $\text{Q}_\text{B}$ . The impact of the proton transfer within the  $\text{Q}_\text{B}$  cluster can be seen in the difference in the size of the negative contour when  $\text{Q}_\text{A}^-$  is formed and when  $\text{Q}_\text{B}^-$  is formed. The smaller increase in negative potential at  $\text{Q}_\text{B}$  is due to the increase in positive potential at Glu L212. The response upon transfer of the electron to  $\text{Q}_\text{A}$  in the presence of  $\text{Q}_\text{B}^-$  is similar to that found for the first reduction of  $\text{Q}_\text{A}$  (cf. Fig. 6 c in comparison to Fig. 6 a). Thus, again the predominant change at neutral pH is around the  $\text{Q}_\text{B}$  site.

Considering all five RC redox states (cf. Fig. 7 a) and excluding protonation of  $\text{Q}_\text{B}$  and Ser L223, almost all of the change in charge induced on the whole protein at neutral pH can be accounted for by the sum of the fractional protonation of the four acidic residues Glu L212, Glu H177, Glu M234, and Asp M43 ( $8.3\text{ \AA}$  away from  $\text{Q}_\text{B}$ ). Allowing Ser L223 to be protonatable has no influence on the results for the first four redox states (i.e., up to and including  $\text{DQ}_\text{A}^- \text{Q}_\text{B}^-$ ; cf. Fig. 7 b compared to Fig. 7 a). In the state  $\text{DQ}_\text{A}\text{Q}_\text{B}^{2-}$ , Ser L223 is protonated at the expense of Asp M43 and, partially, Glu M234 (cf. Fig. 6 e).

## DISCUSSION

One of the main results of these calculations is the characterization of a cluster of strongly coupled ionizable residues around  $\text{Q}_\text{B}$  and its comparison with a cluster near  $\text{Q}_\text{A}$ . The  $\text{Q}_\text{B}$  cluster enables the protein to compensate for the arrival of negative charges on the quinones by proton uptake over

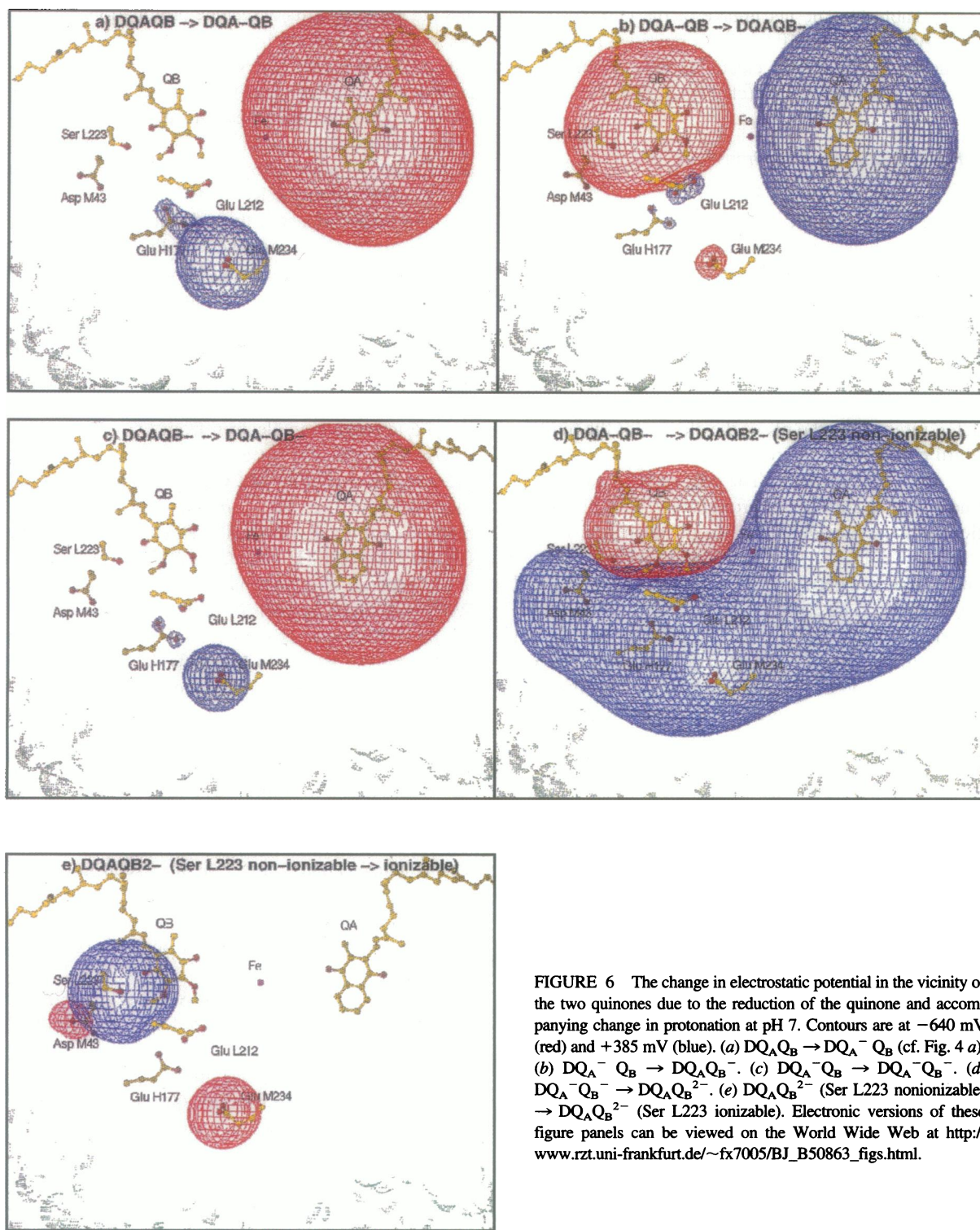


**FIGURE 6** The change in electrostatic potential in the vicinity of the two quinones due to the reduction of the quinone and accompanying change in protonation at pH 7. Contours are at  $-640$  mV (red) and  $+385$  mV (blue). (a)  $DQ_A Q_B \rightarrow DQ_A^- Q_B^-$  (cf. Fig. 4 a). (b)  $DQ_A^- Q_B^- \rightarrow DQ_A^- Q_B^-$ . (c)  $DQ_A^- Q_B^- \rightarrow DQ_A^- Q_B^{2-}$ . (d)  $DQ_A^- Q_B^{2-} \rightarrow DQ_A^- Q_B^{2-}$ . (e)  $DQ_A^- Q_B^{2-}$  (Ser L223 nonionizable)  $\rightarrow DQ_A^- Q_B^{2-}$  (Ser L223 ionizable). Electronic versions of these figure panels can be viewed on the World Wide Web at [http://www.rzt.uni-frankfurt.de/~fx7005/BJ\\_B50863\\_figs.html](http://www.rzt.uni-frankfurt.de/~fx7005/BJ_B50863_figs.html).

a wide pH range, stabilizing reduction of the quinones. The cluster has properties that make some features easier to calculate and others harder to determine than is found for isolated residues. Generally, residues change their protonation state when the redox state is changed in the pH regions where the acid or base is partially ionized. If a strongly coupled di-acid is used as a model for the cluster, the region

of fractional ionization can be expected to extend over a wide pH range. It is relatively easy to estimate the fractional protonation in this range, and this value is not sensitive to the exact value of the first and second pK. However, it is generally very difficult to determine which half of the di-acid is ionized. In the same way, it is likely that the net protonation of the cluster in each redox state and the overall

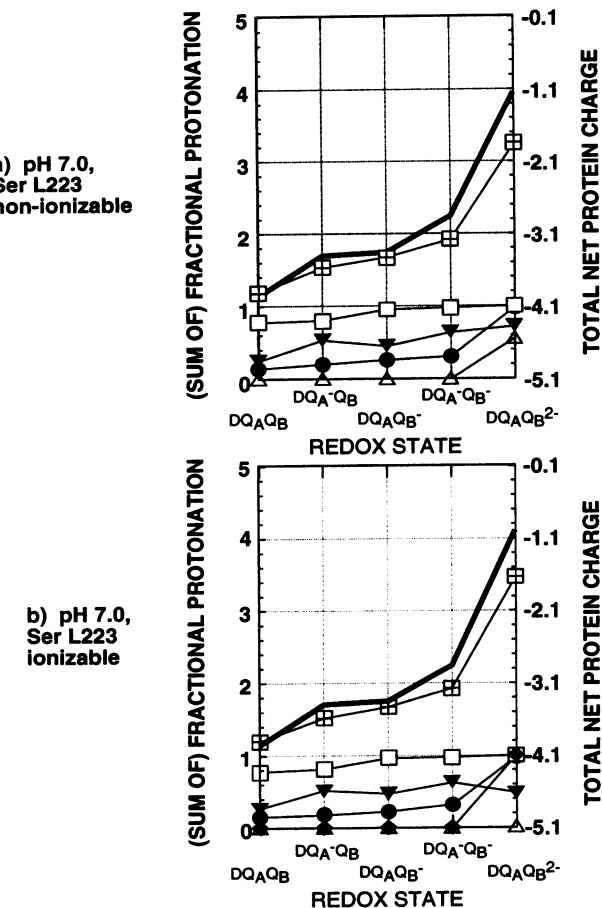


FIGURE 7 Summary: fractional protonation at pH 7.0 as calculated from Monte Carlo sampling for the five residues Asp M43 ( $\triangle$ ), Glu H177 ( $\bullet$ ), Glu L212 ( $\square$ ), Glu M234 ( $\blacktriangledown$ ), and Ser L223 ( $\blacklozenge$ ) in the five different redox states highlighted in Fig. 1. Also plotted is the sum of the protonation of all five residues ( $\blacksquare$ , for the first four redox states this is equivalent to the protonation of the Glu cluster) and the total proton uptake calculated for the whole RC (—).

stoichiometry of proton uptake may be well estimated, whereas there is greater uncertainty in the identification of the residues that play a role at each pH. In addition, the assignment of fractional ionization of residues in the cluster over a wide pH range implies an underlying heterogeneity in any ensemble of RCs. In contrast, the isolated sites are only fractionally protonated in a small pH range near their pK. Errors in estimation of the pK of 1 pH unit are to be expected in the calculations reported here (Yang et al., 1993). This will shift the pH range in which an isolated residue changes protonation state. This may provide the largest source in the error in the total stoichiometry of proton uptake at a each pH.

#### Localization of the Q<sub>B</sub> cluster within the RC

Using a threshold criterion of interaction energies of 2  $\Delta$ pK units (cf. Table 2a), the Q<sub>B</sub> cluster is larger than determined previously in calculations on the RC (Gunner and Honig,

1992; Cometta-Morini et al., 1993; Beroza et al., 1995). Gunner and Honig (1992) employed a criterion of 5  $\Delta$ pK units, whereas Beroza et al. (1995) required that sites have a direct interaction with Q<sub>B</sub><sup>-</sup> of at least 0.8  $\Delta$ pK units. Cometta-Morini et al. (1993) did not give a specific criterion for the presentation of "selected" residues. The location of the Q<sub>B</sub> cluster identified in Table 2 is shown in Fig. 8. It extends for over 33 Å from the solvent-accessible residue His H72 (on the left of Fig. 8 b) to the solvent-accessible amino terminus of the M subunit, Ntr M1 (on the right of Fig. 8 b), thus providing at least two possible entry points for cytoplasmic protons. The maximum distance within the Q<sub>A</sub> cluster is 28 Å (from Arg H86 to Arg M265). Again, there are widely separated residues within this cluster that are solvent accessible. The distance is 25 Å from the solvent-accessible residues Arg H86 to Arg H38, or, from Arg H233 to Glu H61.

#### Why does the Q<sub>A</sub> cluster not contribute to proton uptake at neutral pH?

There is experimental evidence that Q<sub>A</sub> is never directly protonated, whereas Q<sub>B</sub> is only protonated as it becomes doubly reduced (see Okamura and Feher, 1992, for a review). Partial protonation of the surroundings in response to the reduction of the quinone assists in providing a kinetically competent proton donor. As has been presented here, this is the role of the residues in the Q<sub>B</sub> cluster near Q<sub>B</sub>. There is a similar cluster of protonatable residues near Q<sub>A</sub> (cf. Table 3). However, these do not seem to provide the local proton uptake needed to either stabilize a second electron on Q<sub>A</sub> or to allow kinetically competent proton donation to the quinone. The Q<sub>A</sub> and Q<sub>B</sub> clusters are both linked to their protonatable cluster by only one residue, Asp H36 near Q<sub>A</sub> and Glu L212 near Q<sub>B</sub>. These acids are at a similar distance from the quinone and experience large changes in the free energy of protonation when the quinone is ionized. However, Asp H36 is involved in a salt bridge with Arg H33, which stabilizes the charge on the acid so that it remains ionized when Q<sub>A</sub> is reduced. If a second electron were placed on Q<sub>A</sub>, this Asp would now be calculated to become protonated, but this would be coupled to the disruption of the salt bridge to Arg H33. In contrast, Glu L212 is most strongly coupled to two other glutamic acids. The Glu cluster provides a structure that is partially protonated in each redox state and which can therefore bind protons at each stage of quinone reduction. In fact, it appears that it is the Glu cluster near Q<sub>B</sub> that is protonated when Q<sub>A</sub> is reduced. This may provide a mechanism to pre-stabilize electron transfer from Q<sub>A</sub> to Q<sub>B</sub>. In contrast, protonation near Q<sub>A</sub> could provide undesirable stabilization of the electron on Q<sub>A</sub>, which would disfavor electron transfer to Q<sub>B</sub>.

Although the Q<sub>A</sub> and Q<sub>B</sub> clusters have similar numbers of residues, the coupling within the clusters is quite different. Thus, although the structure of the protein shows that there

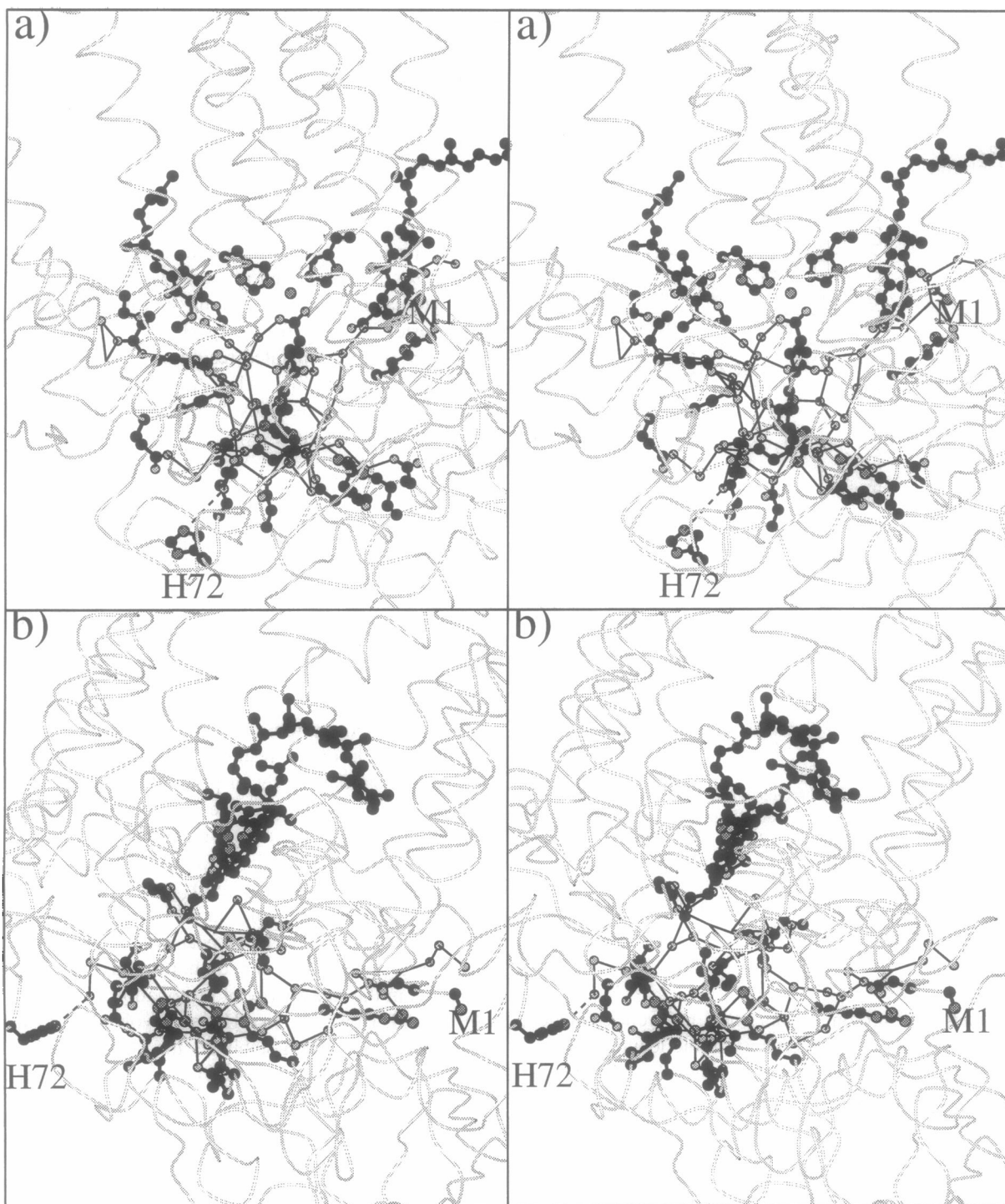


**FIGURE 8** Localization of the  $Q_B$  cluster within the RC. These stereo images were generated with the program MolScript (Kraulis, 1991). The polypeptide backbones are depicted in light gray, with the transmembrane helices in the upper halves of the pictures. The nonheme iron, FeQ,  $Q_A$ ,  $Q_B$ , the nonheme iron ligand His L190, and the residues of the  $Q_B$  cluster are shown in dark gray or black. Also included are the water molecules that are in contact with the residues of the  $Q_B$  cluster, as detailed in Fig. 10. (a) "Classical" view with  $Q_B$  on the left and  $Q_A$  on the right (His H72 front left, Asp M2 back right). (b) Side view of a, slightly tilted clockwise.

are protonatable residues near  $Q_A$ , the electrostatic analysis reveals that the energetics of proton uptake in the two clusters at neutral pH determines that the  $Q_B$  cluster can play an active role in the stabilization of the quinone reduc-

tion, whereas the  $Q_A$  cluster only plays a passive role. This may result from the clusters not being formed from sites that are related by the twofold symmetry between the L and M subunits (Deisenhofer et al., 1995). Thus, the only symme-

try-related cluster sites are Glu L210/Glu M244, Arg L217/Arg M251, and Arg L231/Arg M265. The other contributions from the  $Q_B$  cluster that are in portions of the protein that are identified as homologous at the level of the backbone conformation (Glu L 212 and Glu M261) are changed to nonionizable residues in the  $Q_A$  cluster (Ala M 246, and Leu L227). Other important residues are in the segment M226 to M239, which is not symmetry-related to the L subunit. In addition, residues from the H subunit that caps the cytoplasmic surface of the protein and has different contacts to the L and M subunits play key roles. A revertant of a *Rhodobacter capsulatus* mutant in which the sequence comprising the  $Q_A$  binding site is duplicated and the native  $Q_B$  binding site sequence is deleted ( $Q_AQ_A$  mutant) provides some experimental support for a picture where the protein near  $Q_A$  plays a role that is similar yet distinct from that of the residues near  $Q_B$ . This mutant will support photosynthetic growth (Coleman and Youvan, 1993; further characterized by Li et al., 1995), indicating that although it is possible to deliver electrons to the modified  $Q_B$  site, there are substantial kinetic barriers to the process that may reflect differences in proton transfer.

### Comparison of calculated results with published experimental data

The calculations presented here can be compared with a variety of experimental results. The stoichiometry of proton uptake (cf. Fig. 9) can be compared with experimentally

determined values. The importance of particular residues can in principle be monitored by infrared (IR) spectroscopy (Mäntele, 1993, 1995). In addition, the results of site-directed mutagenesis and second-site revertants can provide evidence for the location of critical residues.

### Comparison of the measured and calculated stoichiometry of proton uptake as a function of pH

Proton uptake by RCs in response to the reduction of  $Q_A$  and  $Q_B$  has been measured by monitoring the solution pH with proton-sensitive dyes (Wraight, 1979; Maroti and Wraight, 1988a), using a pH electrode (McPherson et al., 1988) and by conductometric methods (Maroti and Wraight, 1988a; Maroti, 1993a). These techniques provide a sensitive monitor of the loss of protons from the solution as they are bound by the RCs. However, measurement of proton uptake in *Rp. viridis* RCs is difficult because it is masked by concomitant proton release coupled to oxidation of the cytochrome subunit during re-reduction of the special pair (Maroti, 1993a). Some guidelines can be taken from the more abundant data for the *Rb. sphaeroides* RC (Maroti, 1993a).

### Experimentally measured pH-dependent proton uptake profiles

$DQ_AQ_B \rightarrow DQ_A^-Q_B^-$ . The proton uptake stoichiometry calculated as a function of pH for the transfer of the first

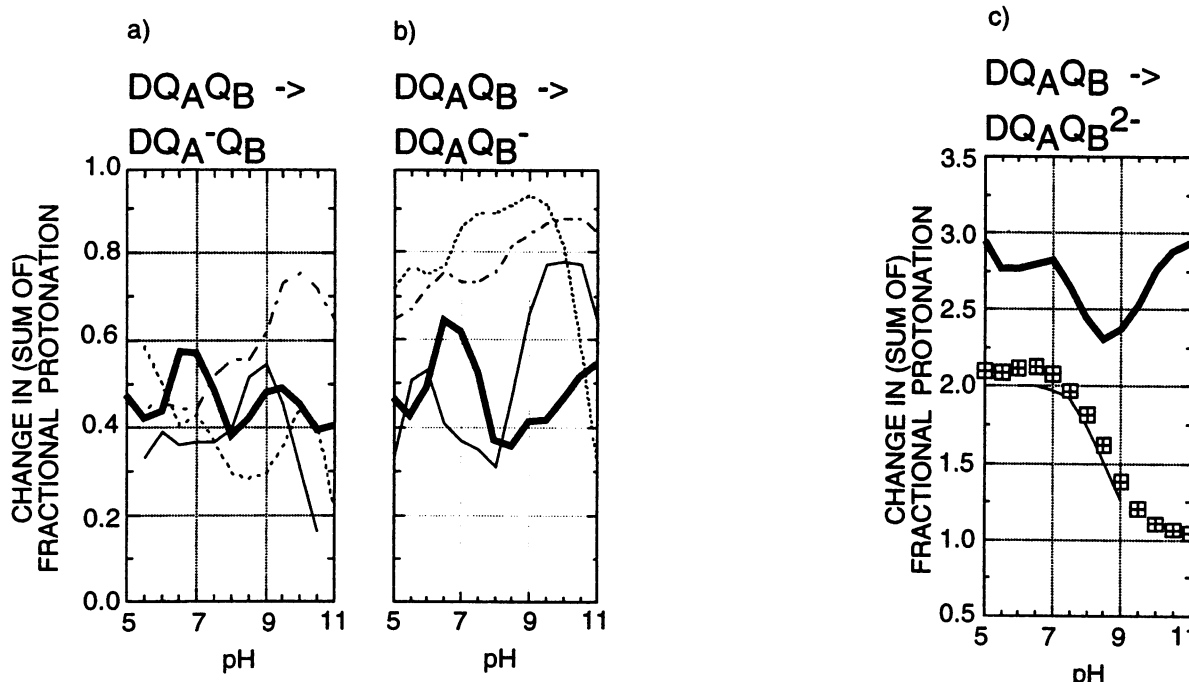


FIGURE 9 Comparison of proton uptake calculated (this study, heavy solid line) and measured for the *Rb. sphaeroides* RC (thin solid line, McPherson et al., 1988, 1993; dotted line, Maroti and Wraight, 1988b). Also plotted in a and b are the calculated profiles for the *Rb. sphaeroides* RC published recently by Beroza et al., 1995 (dotted and dashed line). In the case of c, the calculated uptake for the  $Q_B$  cluster alone (■) is also plotted.

electron to  $Q_A$  is compared with the experimental results for the *Rb. sphaerooides* RC by McPherson et al. (1988) and Maroti and Wright (1988b) in Fig. 9 a. The experimental profile is reproduced reasonably well by our calculations, with errors of less than 0.2 H<sup>+</sup>/RC. At neutral pH, the surplus of approximately +0.2 H<sup>+</sup> can be accounted for by the marginal cytoplasmic sites, and the joint contribution of the  $Q_A$  cluster and the  $Q_B$  cluster of +0.37 H<sup>+</sup> (cf. Fig. 4 c) at pH 7 corresponds very well with the experimental value of McPherson et al. (1988).

$DQ_AQ_B \rightarrow DQ_AQ_B^-$ . The calculated and experimental pH profiles for the transfer of the first electron to  $Q_B$  are compared in Fig. 9 b. The calculated proton uptake is generally smaller than that observed experimentally, with differences ranging from 0.2 to 0.6 H<sup>+</sup>/RC. However, it can be noted that there is also some uncertainty in the experimental results. The *Rb. sphaerooides* data of McPherson et al. (1988) are similar to the data for the *Rp. viridis* RC (Maroti, 1993a), whereas the *Rb. sphaerooides* data of Maroti and Wright (1988b) display considerably higher proton uptake (0.7 to 0.9 H<sup>+</sup>) at lower and medium pH values. The latter results disagree significantly with those obtained more recently by the same laboratory (Shinkarev et al., 1992), which in turn are more similar to those reported by McPherson et al. (1988). We will therefore primarily compare our calculated data with the experimental data of McPherson et al. (1988). The features of the experimental profile with maxima at pH 6 and pH 10 and a minimum at pH 8 are reproduced reasonably well by our calculations, which lie within the experimental extremes from low pH values to pH 9.0. However, at high pH the calculated proton uptake is too low. One possible reason for the discrepancy is that the structure used as a basis for these calculations was determined at pH 6.0 (Lancaster and Michel, manuscript in preparation), and that structural changes may occur at higher pH values (Maroti, 1993b).

$DQ_AQ_B \rightarrow DQ_AQ_B^{2-}$ . It has been a matter of debate (Okamura and Feher, 1992) whether the second electron transfer precedes or follows the uptake of the first proton. Recent deduction of free energy changes associated with the formation of  $Q_BH_2$  indicates that transfer of the second electron to  $Q_B$  precedes the first proton uptake (McPherson et al., 1994). Recent  $Q_A$  substitutions for low potential quinones by the same laboratory (Graige et al., manuscript submitted for publication) have shown the rate of second electron transfer from  $Q_A^-$  to  $Q_B^-$ ,  $k_{AB}^{(2)}$ , to increase with increasing driving force, indicating that electron transfer is the rate-limiting step. This would still be consistent with the existence of  $Q_B^{2-}$  if slow electron transfer were to precede fast proton transfer. However, the authors conclude that their results indicate a mechanism in which rate-limiting electron transfer follows rapid proton transfer, thus disfavoring the existence of  $Q_B^{2-}$ . On the other hand, a  $Q_BH$  intermediate (cf. Fig. 1) has yet to be detected. However, even if  $DQ_AQ_B^{2-}$  is not an intermediate state, the exploration of the changes in RC protonation on formation of  $DQ_AQ_B^{2-}$  remains of interest. The changes in protonation

help to identify the protonatable groups that are far out of equilibrium with the state  $DQ_AQ_B^{2-}$  and so destabilize its formation. In addition, this calculation may provide insight into the groups that are energetically more likely to be transiently protonated on the pathways that provide protons to  $Q_B$ .

In Fig. 9 c the experimental and calculated pH profiles are compared for the transfer of both electrons to  $Q_B$ . The fit of the calculated profile to the data of McPherson et al. (1993) is poor. Although the profile of the contribution of the  $Q_B$  cluster reproduces the experimental data in an excellent manner, the reasons for these two profiles are different. Whereas the experimentally observed drop in proton uptake at higher pH was attributed to the titration of  $Q_BH^-$  with a pK<sub>a</sub> of ~8.5 (McPherson et al., 1993), the calculated profile is effectively determined by the pK<sub>a</sub> of 8.4 for the binding of the third proton in the Glu cluster in the redox state  $DQ_AQ_B^{2-}$  (cf. Fig. 5 a). The latter is clearly not an equilibrium state, because  $Q_B^{2-}$  is rapidly protonated. Nevertheless, the correspondence between the data and calculations indicates that proton transfer into the Glu cluster could be a necessary step for proton and electron transfer to  $Q_B^-$ .

#### Comparison with IR spectroscopic results

Our calculations indicate that proton uptake in response to electron transfer to the quinones is not accomplished by a single site at any pH value. This is consistent with results from IR vibrational spectroscopy, where absorption changes in the region of the protonatable amino acids upon changes in the quinone redox states can be interpreted to indicate that several residues participate in substoichiometric protonation changes. The best characterized residue is Glu L212. An increase in the IR absorption band at 1725(1728) cm<sup>-1</sup> upon  $Q_B^-$  formation has been assigned to the protonation of Glu L212 in *Rb. sphaerooides* RCs (Hienerwadel et al., 1992b, 1995). Changes in this signal are observed for the  $Q_A \rightarrow Q_A^-$ ,  $Q_B \rightarrow Q_B^-$ , and  $Q_A^-Q_B \rightarrow Q_AQ_B^-$  transitions, indicating substoichiometric protonation of Glu L212 for all three transitions. At pH 7.0, our calculations indicate an uptake of +0.02 H<sup>+</sup> on Glu L212 for the  $DQ_AQ_B \rightarrow DQ_A^-Q_B$  transition and an additional +0.15 H<sup>+</sup> for the  $DQ_A^-Q_B \rightarrow DQ_AQ_B^-$  transition. Although quantification of the uptake measured by Fourier transform (FT) IR difference spectroscopy is difficult, proton uptake for the  $DQ_AQ_B \rightarrow DQ_AQ_B^-$  transition in the case of *Rp. viridis* RCs (Breton et al., 1991) is estimated to be half of the 0.3 to 0.6 H<sup>+</sup> determined for *Rb. sphaerooides* RCs (Hienerwadel et al., 1995). In this case, the calculated value of +0.17 H<sup>+</sup> would be consistent with the experimental data. Static FTIR difference measurements in the ground and  $Q_B^-$  states has confirmed that there is less proton uptake by Glu L212 in *Rp. viridis* than in *Rb. sphaerooides* RCs (Breton et al., 1995).

Calculated protonation changes for other acidic residues are qualitatively consistent with currently unassigned sig-

nals in the FTIR difference spectra. In particular, one candidate for the currently unassigned negative signal at 1736  $\text{cm}^{-1}$  in a  $Q_A^- Q_B \rightarrow Q_A Q_B^-$  double difference spectrum on *Rp. viridis* RCs (Hienerwadel et al., 1992a) is Glu M234, which is calculated to release protons upon transfer of the first electron from  $Q_A$  to  $Q_B$  (cf. Fig. 6 b). The general finding that, below pH 8.5, the  $Q_B$  cluster responds more strongly to the reduction of  $Q_A$  than the  $Q_A$  cluster (cf. Fig. 5 a) is consistent with the observation that upon reduction of  $Q_A$  generally the same signals are observed in FTIR difference spectra as for the reduction of  $Q_B$ , but they have smaller amplitude (W. Mäntele, personal communication). With respect to the residue Glu L212, this finding is also consistent with the calculations of Beroza et al. (1995), and experiments by McPherson et al. (1994), Tiede and Hanson (1992), Sebban et al. (1995a), and Maroti et al. (1995) on the RCs of *Rb. sphaeroides* and *Rb. capsulatus*, respectively.

#### Comparison with the behavior of mutant RCs

The work presented here proposes that an extended cluster that includes distant residues is important for proton delivery to the  $Q_B$  site. This picture receives support from revertants where second-site mutations lead to the restoration of photocompetence in mutants incapable of proton transfer. Thus, Arg M231 (Hanson et al., 1993; further characterized by Maroti et al., 1994, and Sebban et al., 1995b) and Arg L231 (Hanson et al., 1995), which are found as second-site mutations in *Rb. capsulatus* RCs, are both located in the  $Q_B$  cluster (cf. Table 2), more than 10 Å (Arg L 231) and 15 Å (Arg M231) from  $Q_B$ , respectively. In particular, Arg M231 is found to be strongly coupled to more than half the residues in the  $Q_B$  cluster (cf. Table 2), and so might play an important role in establishing the electrostatic environment necessary for proton transfer.

Based on the spectroscopic analysis of site-specific mutants of the reaction center from *Rb. sphaeroides* (reviewed by Okamura and Feher, 1992; Takahashi and Wraight, 1994) it was suggested that the first proton to  $Q_B$  is transferred via Asp L213 and Ser L223, and the second via Asp L213 and Glu L212. In *Rp. viridis*, residue L213 is an asparagine. However, its role can apparently be complemented (Rongey et al., 1993) by Asp M43 (which corresponds to Asn M44 in *Rb. sphaeroides*). Relative to the Asp L213 → Asn single mutant, the double mutation Asn M44 → Asp and Asp L213 → Asn in *Rb. sphaeroides* RCs increases  $k^{(1)}_{AB}$  approximately sixfold and  $k^{(2)}_{AB}$  approximately 5000-fold (Rongey et al., 1993), indicating that this residue is far more important for the second electron transfer than for the first. Proton transfer is accelerated by a ratio similar to  $k^{(2)}_{AB}$  (Rongey et al., 1993). Mutation of Asp L210 in *Rb. sphaeroides*, corresponding to Glu L210 in *Rp. viridis* to Asn, has little impact on electron transfer or proton uptake (Paddock et al., 1992). This residue is not found to change its protonation state in the calculations presented here.

A recent mutation of Glu H173 to Gln (Takahashi and Wraight, 1995) in *Rb. sphaeroides*, corresponding to Glu H177 in *Rp. viridis*, has been shown to give rise to a transfer rate for the second electron from  $Q_A$  to  $Q_B$  that is 100-fold slower than in the wild type. This kinetic result corroborates our findings of an important role for Glu H177, especially for proton uptake associated with the transfer of the second electron to  $Q_B$  (see Fig. 7).

#### Comparison to other computational results

Qualitative agreement of the calculated stoichiometry of proton uptake has been found in the calculations of Beroza et al. (1995) on the RC of *Rb. sphaeroides*. However, the calculations presented here seem to fit the experimental profile of McPherson et al. (1988) somewhat better. Although both computational profiles for  $DQ_A Q_B \rightarrow DQ_A^- Q_B$  (cf. Fig. 9 a) are within 0.2 H<sup>+</sup> of the experimental profile of McPherson et al. (1988) between pH 5.5 and 9, the calculations reported here provide a closer match to the experimental data for the reduction of  $Q_B$  between pH 5 and 8.5, with less than 0.25 H<sup>+</sup> deviation (cf. Fig. 9 b). In general, the calculated desolvation penalties, polar interactions, and charge-charge interactions are larger in our study than in the calculations of Beroza et al. (1995) for the *Rb. sphaeroides* RC, and in some cases the difference is large. For instance, the interaction energy between Glu L212 and Glu H173 (Glu H177 in *Rp. viridis*) is reported by Beroza et al. (1995) to be 2.6 ΔpK units, whereas it is 5.4 ΔpK units in Table 2. The effect of decreased desolvation penalties and polar interactions reported by Beroza et al. (1995) approximately cancel in some cases to yield similar pK<sub>int</sub> values (e.g., pK<sub>int</sub>(Glu L212) = 3.7 (Beroza et al., 1995) and pK<sub>int</sub>(Glu L212) = 3.6 (Table 2)). The two sets of calculations have been performed with the same probe radius and the same dielectric constants for solvent and solute. However, the algorithm that defines the surface is different (P. Beroza, personal communication). Somewhat larger electrostatic energies were also reported in earlier calculations on the *Rb. sphaeroides* RC (Gunner and Honig, 1992) using the same methods as described here. Careful consideration of the discrepancies between the work of Beroza et al. (1995) and Gunner and Honig (1992) showed that these were due to differences in coordinates and to the surfacing algorithm.

One significant difference is that Glu M236 (Glu M234 in *Rp. viridis*), which is in the Glu cluster here, is not found to be in the  $Q_B$  cluster in the calculations of Beroza et al. (1995). The reason for this difference is most probably the different conformation of the Glu side chain (Ermler et al., 1994), which in turn is caused by the species differences Gly H73/Arg H70 and Ala H121/Arg H118 (higher numbering refers to *Rp. viridis*), thus causing Glu M236 in the *Rb. sphaeroides* RC to be oriented toward these two Arg residues and away from Glu L212 and Glu H173.

There are three main sources of possible differences between the results reported here and those of Beroza et

al. (1995). First, there are small differences in the amino acid composition of *Rp. viridis* and *Rb. sphaeroides* RCs, notably the Asn L213/Asp M43 and Asp L213/Asn M44 change. Second, the coordinates used by Beroza and co-workers (4RCR; Yeates et al., 1988) are significantly less well defined than the coordinates used for the calculations reported here (cf. Lancaster et al., 1995, for a discussion). Last, there are some differences in the parameters used in the calculations. The partial charges on the quinone and bacteriopheophytin molecules are larger in the calculations presented here (cf. Table 1). The charge distribution on  $\phi_A$  has the largest impact on Glu L104 because the neutral (protonated) form of Glu L104 is stabilized by a hydrogen bond to the ring V keto carbonyl of bacteriopheophytin  $\phi_A$ . In the work of Beroza and co-workers (1995) this residue is reported to titrate in the high pH range with a  $pK_a$  of  $\sim 13$  in the ground state ( $DQ_AQ_B$ ) (Beroza et al., 1995, Fig. 3 a), and some proton uptake by this residue is calculated to occur upon reduction of  $Q_A$  (Beroza et al., 1995, Fig. 4 a). In the calculations reported here, the larger charges on  $\phi_A$  yield more stabilization in the neutral form in  $\Delta G_{pol}$  for this residue. The result is that Glu L104 is calculated to remain fully protonated throughout the pH range studied.

Another difference in the outcome of the two calculations concerns the titration of Arg M247 in *Rb. sphaeroides* (Arg M245 in *Rp. viridis*). Beroza et al. (1995) report an anomalous titration for the ground state  $DQ_AQ_B$ , beginning at pH  $\sim 5$  and ending with  $\sim 20\%$  protonation at pH 15 (cf. Beroza et al., 1995, Fig. 3 a). This leads to the calculation of proton uptake by this residue upon reduction of  $Q_A$  (cf. Beroza et al., 1995, Fig. 4 a). In contrast, this residue is calculated to be fully protonated at all pH values for all redox states in the work reported here. The difference is due to a significantly more favorable  $\Delta G_{pol}$  from backbone dipoles and from the side chain Thr M241/243. This Thr is differently oriented in the two structures. In the best defined structure of the *Rb. sphaeroides* RC (1PCR, Ermler et al., 1994), the Thr M243 side chain has an orientation similar to the structure on which these calculations are based (cf. Lancaster et al., 1995, for a recent comparative discussion of RC x-ray structures).

Instead of a Glu cluster of Glu L212, Glu H177, and Glu M234 (corresponding to Glu L212, H173, and M236 in *Rb. sphaeroides*), Beroza et al. (1995) identify a different cluster of three acidic residues: Glu L212, Asp L213, and Asp L210. A possible reason for the different composition of the cluster is the species difference at position L213, which is Asn in *Rp. viridis*. (vide supra). The inverse titration calculated for Glu L212 in our work is not observed for this residue by Beroza et al. (1995), but instead is observed for Asp L213. In both cases, this inverse titration behavior may be a result of the limitations of computational model (Beroza et al., 1995), although there is some experimental evidence for an anomalous titration behavior of Glu L212 (Hienerwadel et al., 1995).

## Implications for pathways and kinetics of proton transfer

We have calculated the effect of changes in the redox state of the quinone cofactors, as they occur during electron transfer, on the protonation states of the titrating sites in the RC. Stoichiometric proton uptake is only calculated to occur upon transfer of the second electron to  $Q_B^-$ . In contrast to calculations on the transfer of the first electron, those for the second electron are not true equilibrium calculations. This applies especially to the state  $DQ_AQ_B^{2-}$ , where the equilibrium state is for both protons to be bound by the doubly reduced  $Q_B$ . This means that the "equilibrium" protonation uptake calculated for Asp M43/Ser L223 and the Glu cluster will not become fully established before protons are bound by  $Q_B^{2-}$ . Nevertheless, the residues calculated to take up protons upon formation of  $Q_B^{2-}$  are likely candidates for transient protonation upon transfer of the second electron to  $Q_B^-$ . Other participants in the pathways of proton transfer are very likely to be directly or indirectly hydrogen-bonded to these residues. Our findings are summarized in Fig. 10, which includes the residues of the  $Q_B$  cluster and the  $Q_A$  cluster as well as crystallographically determined water molecules.

The residues of the Glu cluster are highlighted with bold frames in Fig. 10, as are Asp M43 and Ser L223. A number of different pathways are possible for protons to reach these five residues from the cytoplasm. The recent observation of a continuous water chain from the cytoplasmic surface to  $Q_B$  in the structure of the RC from *Rb. sphaeroides* (Ermler et al., 1994) implies an involvement of water molecules in the pathway of proton transfer.

Because our calculations do not include water molecules as protonatable groups, it cannot be ruled out that some of the fractional protonation calculated for individual amino acid residues is actually "shared" with adjacent water molecules (cf. Fig. 10). The pathway of proton transfer could include some or possibly all of the water molecules associated with the  $Q_B$  cluster. Two possibilities for protons to enter the RC are either via water W261/Ntr M1 or via His H72. The first pathway would then lead via tightly bound water molecules (cf. Fig. 10) to Asp M2. Because this residue is strongly electrostatically coupled (cf. Table 2) to Asp M230 and Glu H235, the latter two residues could be the next participants in the pathway. From Glu H235, protonation could proceed via Asp H125 and W110 to Glu M234 of the Glu cluster. From Asp M230, protonation of Glu H177 of the Glu cluster could occur. Proton transfer within the Glu cluster is possible via the two tightly bound water molecules W187 and W92. The second pathway via His H72 would require proton transfer via one or two disordered water molecules and further ordered water molecules to Glu M234, to which it is coupled. These two pathways involve amino acid residues solely of the  $Q_B$  cluster. Other pathways are possible if additional disordered water mol-

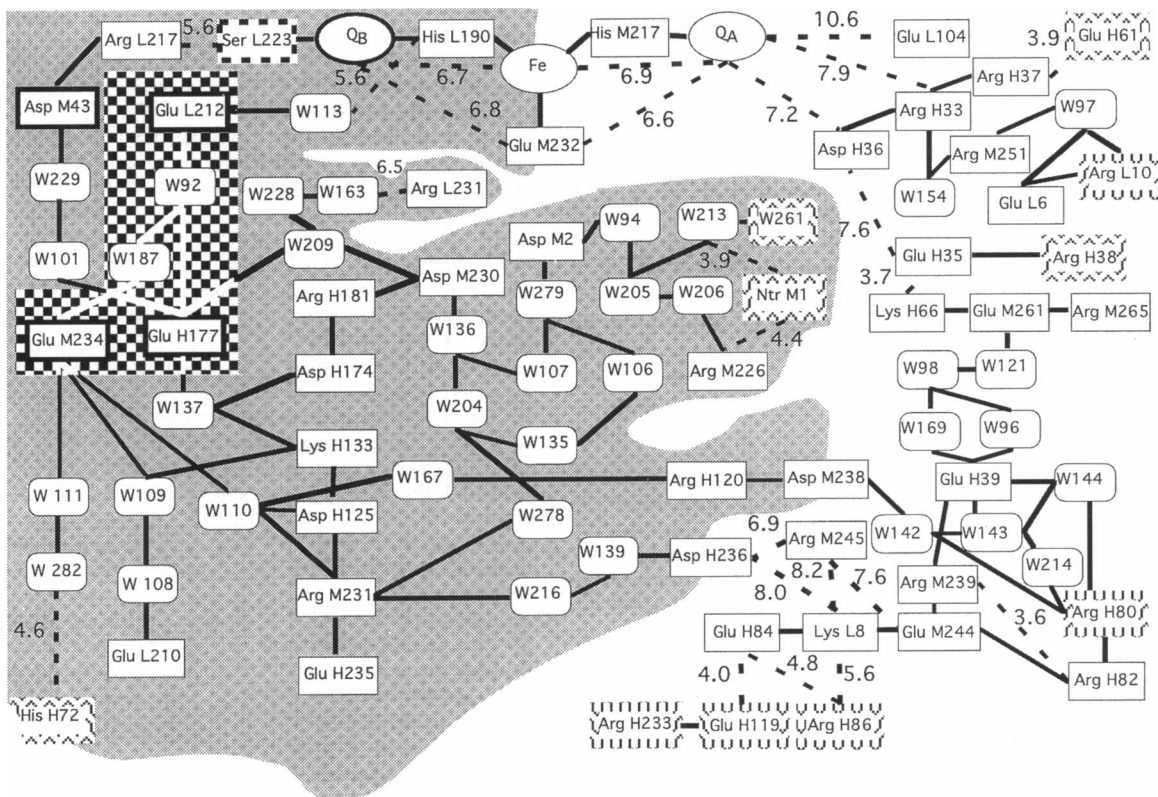


**FIGURE 10** Schematic diagram of residues identified in Tables 2 and 3. This diagram includes water molecules identified in the x-ray structure of the quinone-reconstituted RC (Lancaster and Michel, manuscript in preparation). Waters with numbers greater than 162 were not identified in the structure of Deisenhofer et al. (1995). Solid lines (—) link residues and water molecules that are within hydrogen bonding distance ( $<3.5\text{ \AA}$ ). Dashed lines (---) designate longer distances (explicitly given in angstroms). Bold frames highlight the five residues identified in Fig. 7. Frames with wave patterns designate residues that are at least partially solvent exposed (i.e.,  $1.2\text{ \AA}$  or less from the solvent accessible surface); cf. Tables 2 and 3). The gray background defines the  $Q_B$  cluster (cf. Table 2), the white background the  $Q_A$  cluster (cf. Table 3).

ecules are assumed to be part of them, or if members of the  $Q_A$  cluster are considered to be directly involved.

Transfer of a proton from Glu H177 in the Glu cluster to Asp M43 coupled via water molecules W101 and W229 is straightforward. Through transfer of the proton from Asp M43 via a disordered water molecule, protonation of Ser L223 could occur in the state  $DQ_A^-Q_B^{2-}$ . This residue has been shown to be involved in stabilizing the reduced quinone and in efficient donation of the first proton to the distal oxygen of  $Q_B$  in the *Rp. viridis* RC (Leibl et al., 1993) and the *Rb. sphaeroides* RC (Paddock et al., 1990). The second proton could then be transferred from Glu L212 (Okamura and Feher, 1992; McPherson et al., 1994), probably via water W113 and one or two disordered water molecules, to the proximal quinolate oxygen.

## CONCLUSION

The work presented here demonstrates how light-induced electron transfer is coupled to the uptake of protons and how electrostatic calculations can help to identify amino acid residues that are possibly involved in proton uptake to the  $Q_B$  site. A strongly interacting cluster of the three Glu

residues L212, H177, and M234 near  $Q_B$  accounts for the net effect of this charge compensation at neutral pH for all redox transitions up to and including the diradical state  $DQ_A^-Q_B^-$ . This Glu cluster is part of a larger interacting network of ionizable residues around  $Q_B$  ( $Q_B$  cluster) that extends to the solvent accessible surface. An analogous cluster of ionizable residues around  $Q_A$  ( $Q_A$  cluster) has different electrostatic properties. In particular, it is not so strongly coupled and apparently is not involved in proton uptake at neutral pH. The fit of the calculated data to experimental results is better than in previous publications. The calculated complex titration behavior of the strongly interacting residues of the  $Q_B$  cluster may be a common feature in proton-transferring membrane proteins.

We thank Anthony Nicholls for timely and continuing modifications of DelPhi and GRASP; Paul Beroza, Jacques Breton, Mark Paddock, and Mike Graige for making manuscripts available before publication; Rainer Hienerwadel for providing a copy of his Ph.D. thesis (1993) before publication of the manuscript of Hienerwadel et al. (1995); and Laura Baciu for discussions. We thank George Feher, Mel Okamura, Mark Paddock, and Paul Beroza for careful reading of the manuscript.

We acknowledge the support of the Max-Planck-Gesellschaft (CRDL and HM), and of National Institutes of Health grant GM-48726 (MRG) and NSF grant MCB-9304127 (BH).

## REFERENCES

- Antosiewicz, J., J. A. McCammon, and M. K. Gilson. 1994. Prediction of pH-dependent properties of proteins. *J. Mol. Biol.* 238:415–436.
- Bashford, D., and K. Gerwert. 1992. Electrostatic calculations of the pK<sub>a</sub>'s of ionizable groups in bacteriorhodopsin. *J. Mol. Biol.* 224:473–486.
- Bashford, D., and M. Karplus. 1990. pK<sub>a</sub>s of ionizable groups in proteins: atomic detail from a continuum electrostatic model. *Biochemistry*. 29: 10219–10225.
- Beroza, P. 1993. Electrostatic interactions in proteins: application to the photosynthetic reaction center. Ph.D. thesis. University of California, San Diego.
- Beroza, P., D. R. Fredkin, M. Y. Okamura, and G. Feher. 1991. Protonation of interacting residues in a protein by a Monte Carlo method: application to lysozyme and the photosynthetic reaction center of *Rhodobacter sphaeroides*. *Proc. Natl. Acad. Sci. USA*. 88:5804–5808.
- Beroza, P., D. R. Fredkin, M. Y. Okamura, and G. Feher. 1995. Electrostatic calculations of amino acid titration and electron transfer, Q<sub>A</sub><sup>-</sup>Q<sub>B</sub> → Q<sub>A</sub>Q<sub>B</sub><sup>-</sup>, in the reaction center. *Biophys. J.* 68:2233–2250.
- Breton, J., C. Berthomieu, D. L. Thibodeau, and E. Nabedryk. 1991. Probing the secondary quinone (Q<sub>B</sub>) environment in photosynthetic bacterial reaction centers by light-induced FTIR difference spectroscopy. *FEBS Lett.* 288:109–113.
- Breton, J., C. Boullais, G. Berger, C. Mioskowski, and E. Nabedryk. 1995. Binding sites of quinones in photosynthetic bacterial reaction centers investigated by light-induced FTIR difference spectroscopy: symmetry of the carbonyl interactions and close equivalence of the Q<sub>B</sub> vibrations in *Rhodobacter sphaeroides* and *Rhodopseudomonas viridis* probed by isotope labeling. *Biochemistry*. 34:11606–11616.
- Brooks, B. R., R. E. Brucolieri, B. D. Olafson, D. J. States, S. Swaminathan, and M. Karplus. 1983. CHARMM: A program for macromolecular energy, minimization, and dynamics calculation. *J. Comp. Chem.* 4:187–217.
- Carithers, R. P., and W. W. Parson. 1975. Delayed fluorescence from *Rhodopseudomonas viridis* following single flashes. *Biochim. Biophys. Acta*. 387:194–211.
- Coleman, W. J., and D. C. Youvan. 1993. Atavistic reaction centre. *Nature*. 366:517–518.
- Cometta-Morini, C., C. Scharnagl, and S. F. Fischer. 1993. Proton transfer to ubiquinone Q<sub>B</sub> in the photosynthetic reaction center of *Rps. viridis*: the role of electrostatic interactions. *Int. J. Quant. Chem. Quant. Biol. Symp.* 20:89–106.
- Connolly, M. L. 1983. Analytical molecular surface calculation. *J. Appl. Crystallogr.* 16:548–558.
- Cramer, W. A., and D. B. Knaff. 1991. Energy Transduction in Biological Membranes. A Textbook of Bioenergetics. Springer Verlag, New York.
- Crofts, A. R., and C. A. Wright. 1983. The electrochemical domain of photosynthesis. *Biochim. Biophys. Acta*. 726:149–185.
- Deisenhofer, J., O. Epp, K. Miki, R. Huber, and H. Michel. 1985. Structure of the protein subunits in the photosynthetic reaction centre of *Rhodopseudomonas viridis* at 3 Å resolution. *Nature*. 318:618–624.
- Deisenhofer, J., O. Epp, I. Sning, and H. Michel. 1995. Crystallographic refinement at 2.3 Å resolution and refined model of the photosynthetic reaction center from *Rhodopseudomonas viridis*. *J. Mol. Biol.* 246: 429–457.
- Deisenhofer, J., and H. Michel. 1989. The photosynthetic reaction centre from the purple bacterium *Rhodopseudomonas viridis*. *EMBO J.* 8:2149–2169.
- Dracheva, S. M., L. A. Drachev, A. A. Konstantinov, A. Yu. Semenov, V. P. Skulachev, A. M. Arutjunjan, V. A. Shuvalov, and S. M. Zaberezhnaya. 1988. Electrogenic steps in the redox reactions catalyzed by photosynthetic reaction-centre complex from *Rhodopseudomonas viridis*. *Eur. J. Biochem.* 171:253–264.
- Ermler, U., G. Fritzsch, S. K. Buchanan, and H. Michel. 1994. Structure of the photosynthetic reaction centre from *Rhodobacter sphaeroides* at 2.65 Å resolution: cofactors and protein-cofactor interactions. *Structure*. 2:925–936.
- Fritzsch, G., S. K. Buchanan, and H. Michel. 1989. Assignment of cytochrome hemes in crystallized reaction centers from *Rhodopseudomonas viridis*. *Biochim. Biophys. Acta*. 977:157–162.
- Gao, J.-L., R. J. Shope, and C. A. Wright. 1990. Charge recombination between the oxidized high-potential c-type cytochromes and QA in reaction centers from *Rhodopseudomonas viridis*. *Biochim. Biophys. Acta*. 1015:96–108.
- Gilson, M. K., and B. Honig. 1986. The dielectric constant of a folded protein. *Biopolymers*. 25:2097–2119.
- Gilson, M. K., K. A. Sharp, and B. Honig. 1987. Calculating the electrostatic potential of molecules in solution: method and error assessment. *J. Comp. Chem.* 9:327–335.
- Gunner, M. R., and B. Honig. 1991. Electrostatic control of midpoint potentials in the cytochrome subunit of the *Rhodopseudomonas viridis* reaction center. *Proc. Natl. Acad. Sci. USA*. 88:9151–9155.
- Gunner, M. R., and B. Honig. 1992. Calculations of proton uptake in *Rb. sphaeroides* reaction centers. In *The Photosynthetic Bacterial Reaction Center II*. J. Breton and A. Verméglio, editors. Plenum Press, New York. 403–410.
- Hanson, D. K., Y.-L. Deng, P. Sebban, and M. Schiffer. 1995. Compensation for L212Glu in bacterial reaction centers. *Photosynth. Res. Suppl.* 1:72. (Abstr.)
- Hanson, D. K., D. M. Tiede, S. L. Nance, C.-H. Chang, and M. Schiffer. 1993. Site specific and compensatory mutations imply unexpected pathways for proton delivery to the Q<sub>B</sub> binding site of the photosynthetic reaction center. *Proc. Natl. Acad. Sci. USA*. 90:8929–8933.
- Harvey, S. C. 1989. Treatment of electrostatic effects in macromolecular modeling. *Proteins*. 5:78–92.
- Hienerwadel, R., S. Grzybek, C. Fogel, W. Kreutz, M. Y. Okamura, M. L. Paddock, J. Breton, E. Nabedryk, and W. Mantele. 1995. Protonation of Glu L212 following Q<sub>B</sub><sup>-</sup> formation in the photosynthetic reaction center of *Rhodobacter sphaeroides*: evidence from time-resolved infrared spectroscopy. *Biochemistry*. 34:2832–2843.
- Hienerwadel, R., E. Nabedryk, J. Breton, W. Kreutz, and W. Mantele. 1992a. Time-resolved infrared and static FTIR studies of Q<sub>A</sub> → Q<sub>B</sub> electron transfer in *Rp. viridis* reaction centers. In *The Photosynthetic Bacterial Reaction Center II*. J. Breton and A. Verméglio, editors. Plenum Press, New York. 163–172.
- Hienerwadel, R., E. Nabedryk, M. L. Paddock, S. Rongey, M. Y. Okamura, W. Mantele, and J. Breton. 1992b. Proton transfer mutants of *Rb. Sphaeroides*: characterization of reaction centers by infrared spectroscopy. In *Research in Photosynthesis*, Vol. 1. N. Murata, editor. Kluwer Academic Publishers, Dordrecht, The Netherlands. 437–440.
- Hoff, A. J. 1988. Nomen est omen. A note on nomenclature. In *The Photosynthetic Bacterial Reaction Center: Structure and Dynamics*. J. Breton and A. Verméglio, editors. Plenum Press, New York. 98–99.
- Holzapfel, W., U. Finkle, W. Kaiser, D. Oesterhelt, H. Scheer, H. U. Stitz, and W. Zinth. 1989. Observation of a bacteriochlorophyll anion radical during the primary charge separation in a reaction center. *Chem. Phys. Lett.* 160:1–7.
- Honig, B., and A. Nicholls. 1995. Classical electrostatics in biology and chemistry. *Science*. 268:1144–1149.
- IUPAC-IUB Commission on Biochemical Nomenclature. 1975. Nomenclature of quinones with isoprenoid side chains. Recommendations 1973. *Eur. J. Biochem.* 53:15–18.
- IUPAC-IUB Joint Commission on Biochemical Nomenclature. 1984. Nomenclature and symbolism for amino acids and peptides. Recommendations 1983. *Eur. J. Biochem.* 138:9–37.
- Kirmaier, C., and D. Holten. 1993. Electron transfer and charge recombination reactions in wild-type and mutant bacterial reaction centers. In *The Photosynthetic Reaction Center*, Vol. 2. J. Deisenhofer and J. Norris, editors. Academic Press, San Diego. 49–70.
- Knaff, D. B. 1993. The cytochrome bc<sub>1</sub> complexes of photosynthetic purple bacteria. *Photosynth. Res.* 35:117–133.
- Kraulis, P. J. 1991. MolScript, a program to produce both detailed and schematic plots of protein structures. *J. Appl. Crystallogr.* 24:946–950.
- Lancaster, C. R. D., U. Ermler, and H. Michel. 1995. The structures of photosynthetic reaction centers from purple bacteria as revealed by x-ray crystallography. In *Anoxygenic Photosynthetic Bacteria*. R. E. Blankens-

- ship, M. T. Madigan, and C. E. Bauer, editors. Kluwer Academic Publishers, Dordrecht, The Netherlands. 503–526.
- Lancaster, C. R. D., and H. Michel. 1996. New insights into the x-ray structure of the reaction center from *Rhodopseudomonas viridis*. In Reaction Centers of Photosynthetic Bacteria. Structure and Dynamics. Proceedings of the Feldafing III Workshop. M. E. Michel-Beyerle, editor. Springer-Verlag, Berlin. 23–36.
- Leibl, W., and J. Breton. 1991. Kinetic properties of the acceptor quinone complex in *Rhodopseudomonas viridis*. *Biochemistry*. 30:9634–9642.
- Leibl, W., I. Sinning, G. Ewald, H. Michel, and J. Breton. 1993. Evidence that serine L223 is involved in the proton transfer pathway to Q<sub>B</sub> in the photosynthetic reaction center from *Rhodopseudomonas viridis*. *Biochemistry*. 32:1958–1964.
- Li, J., W. J. Coleman, D. C. Youvan, and M. R. Gunner. 1995. Characterization of a *Rhodobacter capsulatus* RC symmetrized mutant with the Q<sub>B</sub> site made more like Q<sub>A</sub>. *Photosynth. Res. Suppl.* 1:65. (Abstr.)
- Mantele, W. 1993. Infrared vibrational spectroscopy of the photosynthetic reaction center. In The Photosynthetic Reaction Center, Vol. 2. J. Deisenhofer and J. Norris, editors. Academic Press, San Diego. 239–283.
- Mantele, W. 1995. Infrared vibrational spectroscopy of reaction centers. In Anoxygenic Photosynthetic Bacteria. R. E. Blankenship, M. T. Madigan, and C. E. Bauer, editors. Kluwer Academic Publishers, Dordrecht, The Netherlands. 627–647.
- Maroti, P. 1993a. Flash-induced proton transfer in photosynthetic bacteria. *Photosynth. Res.* 37:1–17.
- Maroti, P. 1993b. Use of Marcus theory of electron transfer as an intramolecular ruler. *J. Photochem. Photobiol. B Biol.* 19:235–238.
- Maroti, P., D. K. Hanson, L. Baciou, M. Schiffer, and P. Sebban. 1994. Proton conduction within the reaction centers of *Rhodobacter capsulatus*: the electrostatic role of the protein. *Proc. Natl. Acad. Sci. USA*. 91:5617–5621.
- Maroti, P., D. K. Hanson, M. Schiffer, and P. Sebban. 1995. Long range electrostatic interaction in the bacterial photosynthetic reaction centre. *Nature Struct. Biol.* 2:1057–1059.
- Maroti, P., and C. A. Wright. 1988a. Flash-induced H<sup>+</sup> binding by bacterial photosynthetic reaction centers: comparison of spectrophotometric and conductometric methods. *Biochim. Biophys. Acta*. 934: 314–328.
- Maroti, P., and C. A. Wright. 1988b. Flash-induced H<sup>+</sup> binding by bacterial photosynthetic reaction centers: influences of the redox states of the acceptor quinones and primary donor. *Biochim. Biophys. Acta*. 934:329–347.
- Mathis, P., I. Sinning, and H. Michel. 1992. Kinetics of electron transfer from the primary to the secondary quinone in *Rhodopseudomonas viridis*. *Biochim. Biophys. Acta*. 1098:151–158.
- McPherson, P. H., M. Y. Okamura, and G. Feher. 1988. Light-induced proton uptake by photosynthetic reaction centers from *Rb. sphaeroides* R-26. I. Protonation of the one-electron states D<sup>+</sup>Q<sub>A</sub><sup>-</sup>, DQ<sub>A</sub><sup>-</sup>, D<sup>+</sup>Q<sub>A</sub>Q<sub>B</sub><sup>-</sup>, and DQ<sub>A</sub>Q<sub>B</sub><sup>-</sup>. *Biochim. Biophys. Acta*. 934:348–368.
- McPherson, P. H., M. Y. Okamura, and G. Feher. 1990. Electron transfer from the reaction center of *Rhodobacter sphaeroides* to the quinone pool: doubly reduced Q<sub>B</sub> leaves the reaction center. *Biochim. Biophys. Acta*. 1016:289–292.
- McPherson, P. H., M. Y. Okamura, and G. Feher. 1993. Light-induced proton uptake by photosynthetic reaction centers from *Rhodobacter sphaeroides* R-26. II. Protonation of the state DQ<sub>A</sub>Q<sub>B</sub><sup>2-</sup>. *Biochim. Biophys. Acta*. 1144:309–324.
- McPherson, P. H., M. Schönfeld, M. L. Paddock, M. Y. Okamura, and G. Feher. 1994. Protonation and free energy changes associated with formation of Q<sub>B</sub>H<sub>2</sub> in native and Glu-L212 → Gln mutant reaction centers from *Rhodobacter sphaeroides*. *Biochemistry*. 33:1181–1193.
- Mitchell, P. 1979. Keilin's respiratory chain concept and its chemiosmotic consequences. *Science*. 206:1148–1159.
- Nagle, J. F., and S. Tristam-Nagle. 1983. Hydrogen bonded chain mechanisms for proton conduction and proton pumping. *J. Membr. Biol.* 74:1–14.
- Nicholls, A., and B. Honig. 1991. A rapid finite difference algorithm, utilizing successive over-relaxation to solve the Poisson-Boltzmann equation. *J. Comp. Chem.* 12:435–445.
- Nicholls, A., K. A. Sharp, and B. Honig. 1991. Protein folding and association: insights from the interfacial and thermodynamic properties of hydrocarbons. *Proteins*. 11:281–296.
- Nicholls, D. G., and S. J. Ferguson. 1992. Bioenergetics 2. Academic Press, London.
- Okamura, M. Y., and G. Feher. 1992. Proton transfer in reaction centers from photosynthetic bacteria. *Annu. Rev. Biochem.* 61:861–869.
- Okamura, M. Y., and G. Feher. 1995. Proton-coupled electron transfer reactions of Q<sub>B</sub> in reaction centers from photosynthetic bacteria. In Anoxygenic Photosynthetic Bacteria. R. E. Blankenship, M. T. Madigan, and C. E. Bauer, editors. Kluwer Academic Publishers, Dordrecht, The Netherlands. 577–594.
- Paddock, M. L., A. Juth, G. Feher, and M. Y. Okamura. 1992. Electrostatic effects of replacing Asp-L210 with Asn in bacterial RCs from *Rb. sphaeroides*. *Biophys. J.* 61:153a. (Abstr.)
- Paddock, M. L., P. H. McPherson, G. Feher, and M. Y. Okamura. 1990. Pathway of proton transfer in bacterial reaction centers: replacement of serine-L223 by alanine inhibits electron and proton transfers associated with reduction of quinone to dihydroquinone. *Proc. Natl. Acad. Sci. USA*. 87:6803–6807.
- Parson, W. W. 1978. Quinones as secondary electron acceptors. In The Photosynthetic Bacteria. R. K. Clayton and W. R. Sistrum, editors. Plenum Press, New York. 455–469.
- Parson, W. W., and B. Ke. 1982. Primary photochemical reactions. In Photosynthesis: Energy Conversion by Plants and Bacteria, Vol. 1. Govindjee, editor. Academic Press, New York. 331–385.
- Richards, F. M. 1977. Areas, volumes, packing, and protein structure. *Annu. Rev. Biophys. Bioeng.* 6:151–176.
- Rongey, S. H., M. L. Paddock, G. Feher, and M. Y. Okamura. 1993. Pathway of proton transfer in bacterial reaction centers: second-site mutation Asn M44 213 Asp restores electron and proton transfer in reaction centers from the photosynthetically deficient Asp L213→Asn mutant of *Rhodobacter sphaeroides*. *Proc. Natl. Acad. Sci. USA*. 90: 1325–1329.
- Sampogna, R. V., and B. Honig. 1994. Environmental effects on the protonation states of active site residues in bacteriorhodopsin. *Biophys. J.* 66:1341–1352.
- Sebban, P., P. Maroti, and D. K. Hanson. 1995a. Electron and proton transfer to the quinones in bacterial photosynthetic reaction centers: insight from combined approaches of molecular genetics and biophysics. *Biochimie*. 77:677–694.
- Sebban, P., P. Maroti, M. Schiffer, and D. K. Hanson. 1995b. Electrostatic dominoes: long distance propagation of mutational effects in photosynthetic reaction centers of *Rhodobacter capsulatus*. *Biochemistry*. 34: 8390–8397.
- Sharp, K. A., and B. Honig. 1990. Electrostatic interactions in macromolecules: theory and applications. *Annu. Rev. Biophys. Biophys. Chem.* 19:301–332.
- Shinkarev, V. P., E. Takahashi, and C. A. Wright. 1992. Electrostatic interactions and flash-induced proton uptake in reaction centers from *Rb. sphaeroides*. In The Photosynthetic Bacterial Reaction Center II. J. Breton and A. Verméglio, editors. Plenum Press, New York. 375–387.
- Shinkarev, V. P., and C. A. Wright. 1993. Electron and proton transfer in the acceptor quinone complex of reaction centers of Phototrophic Bacteria. In The Photosynthetic Reaction Center, Vol. 1. J. Deisenhofer and J. Norris, editors. Academic Press, San Diego. 193–255.
- Sudmeier, J. L., and C. N. Reilly. 1964. Nuclear magnetic resonance studies of protonation of polyamine and aminocarboxylate compounds in aqueous solution. *Anal. Chem.* 36:1698–1706.
- Takahashi, E., and C. A. Wright. 1994. Molecular genetic manipulation and characterization of mutant photosynthetic reaction centers from purple non-sulfur bacteria. *Adv. Mol. Cell Biol.* 10:197–251.
- Takahashi, E., and C. A. Wright. 1995. Site-directed mutagenesis of the H subunit residue Glu H173 of the photosynthetic reaction center from *Rhodobacter sphaeroides*. *Biophys. J.* 68:A95. (Abstr.)
- Tanford, C., and J. G. Kirkwood. 1957. Theory of protein titration curves I. General equations for impenetrable spheres. *J. Am. Chem. Soc.* 79: 5333–5339.
- Tiede, D. M., and D. K. Hanson. 1992. Protein relaxation following quinone reduction in *Rb. capsulatus*: detection of likely protonation-linked opti-

- cal absorbance changes of the chromatophores. In *The Photosynthetic Bacterial Reaction Center II*. J. Breton and A. Verméglia, editors. Plenum Press, New York. 341–350.
- Treutlein, H., K. Schulten, A. T. Brünger, M. Karplus, J. Deisenhofer, and H. Michel. 1992. Chromophore protein interactions and the function of the photosynthetic reaction center: a molecular dynamics study. *Proc. Natl. Acad. Sci. USA*. 89:75–79.
- Warshel, A., and S. Russell. 1984. Calculation of electrostatic interactions in biological systems and in solution. *Q. Rev. Biophys.* 17:283–422.
- Warwicker, J., and H. C. Watson. 1982. Calculation of the electric potential in the active site cleft due to  $\alpha$ -helix dipoles. *J. Mol. Biol.* 157: 671–679.
- Welte, W., H. Hüdig, T. Wacker, and W. Kreutz. 1983. Chromatofocusing as a simple method of purification of two bacterial photosynthetic proteins: cytochrome  $c_2$  and reaction centre of *Rhodopseudomonas viridis*. *J. Chromatogr.* 259:341–346.
- Weyer, K. A., W. Schäfer, F. Lottspeich, and H. Michel. 1987. The cytochrome subunit of the photosynthetic reaction center from *Rhodopseudomonas viridis* is a lipoprotein. *Biochemistry*. 26:2909–2914.
- Wraight, C. A. 1979. Electron acceptors of bacterial photosynthetic reaction centers. II.  $H^+$  Binding coupled to secondary electron transfer in the quinone acceptor complex. *Biochim. Biophys. Acta*. 548:309–327.
- Wraight, C. A. 1982. The involvement of stable semiquinones in the two-electron gates of plant and bacterial photosystems. In *Function of Quinones in Energy Conserving Systems*. B. L. Trumpower, editor. Academic Press, New York. 181–197.
- Yang, A.-S., M. R. Gunner, R. Sampogna, K. Sharp, and B. Honig. 1993. On the calculation of  $pK_a$ s in proteins. *Proteins*. 15:252–265.
- Yeates, T. O., H. Komiya, A. Chirino, D. C. Rees, J. P. Allen, and G. Feher. 1988. Structure of the reaction center from *Rhodobacter sphaeroides R-26* and 2.4.1: protein-cofactor (bacteriochlorophyll, bacteriopheophytin, and carotenoid) interactions. *Proc. Natl. Acad. Sci. USA*. 85:7993–7997.
- Zinth, W., and W. Kaiser. 1993. Time-resolved spectroscopy of the primary electron transfer in reaction centers of *Rhodobacter sphaeroides* and *Rhodopseudomonas viridis*. In *The Photosynthetic Reaction Center*, Vol. 2. J. Deisenhofer and J. Norris, editors. Academic Press, San Diego. 71–88.